

APPENDIX C

KORACIN, D., FRYE, J., AND V. ISAKOV, 1999. A METHOD OF EVALUATING
ATMOSPHERIC MODELS USING TRACER MEASUREMENTS, ACCEPTED FOR PUBLICATION
IN THE *JOURNAL OF APPLIED METEOROLOGY*

A METHOD OF EVALUATING ATMOSPHERIC MODELS USING TRACER MEASUREMENTS

Darko Koracin¹ and James Frye

Desert Research Institute, Reno, Nevada

Vlad Isakov

DynTel, Research Triangle Park, North Carolina

Accepted for publication in the *Journal of Applied Meteorology*

22 January 1999

¹Corresponding author address: Dr. Darko Koracin, Desert Research Institute, 2215 Raggio Parkway, Reno, NV 89512
E-mail: darko@dri.edu

A METHOD OF EVALUATING ATMOSPHERIC MODELS USING TRACER MEASUREMENTS

Darko Koracin and James Frye

Desert Research Institute, Reno, Nevada

Vlad Isakov

DynTel, Research Triangle Park, North Carolina

ABSTRACT

We have developed a method that uses tracer measurements as the basis for comparing and evaluating wind fields. An important advantage of the method is that the wind fields are evaluated from the tracer measurements without introducing dispersion calculations. The method can be applied to wind fields predicted by different atmospheric models or to wind fields obtained from interpolation and extrapolation of measured data. The method uses a cost function to quantify the success of wind fields in representing tracer transport. A cost function, "tracer potential", is defined to account for the magnitude of the tracer concentration at the tracer receptors and the separation between each segment of a trajectory representing wind field transport and each of the tracer receptors. The tracer potential resembles a general expression for a physical potential because the success of a wind field trajectory is directly proportional to the magnitude of the tracer concentration and inversely proportional to its distance from this concentration. A reference tracer potential is required to evaluate the relative success of the wind fields and is defined by the initial location of any trajectory at the source. Then the method is used to continuously calculate the tracer potential along each trajectory as determined by the wind fields in time and space. Increased potential relative to the reference potential along the trajectory indicates good performance of the wind fields and vice versa. If there is sufficient spatial coverage of near and far receptors around the source, then the net tracer potential area can be used to infer the overall success of the wind fields. If there are mainly near-source receptors, then the positive tracer potential area should be used. If the vertical velocity of the wind fields is not available, then the success of the wind fields can be estimated from the vertically-integrated area under the tracer potential curve. A trajectory with a maximum tracer potential is constructed for each daily tracer measurement, and this tracer potential is used to normalize the relative success of the wind fields in reproducing the transport of tracers. The method is not sensitive to the exact form of the cost function because a test with an inverse square-root dependence in the cost function rather than an inverse linear distance dependence ranked the wind fields in the same order. The method requires sufficient spatial coverage of tracer receptors in the vicinity of a source and primarily gives credit to the wind fields that are able to approach areas with high tracer concentrations. The method can quantitatively determine which wind fields are best able to reproduce the main transport of tracers and can be used to determine the most successful wind fields to serve as a solid base for necessary improvement of dispersion models. It can also be used as a screening method prior to using dispersion models. Since the measured tracer concentrations

are affected by both transport and dispersion, however, the method does not evaluate the capabilities of successful wind fields, as input to dispersion algorithms, to create tracer concentrations at receptors that are similar to measured ones. The tracer potential method has been applied to data from a comprehensive field program that included tracer measurements and was conducted in the Colorado River Valley area in the southwest U.S. in 1992. Wind fields obtained from four atmospheric models as well as those derived from the wind profiler measurements were tested, and the results of their comparison are presented. Since data from the tracer experiment are publicly available, this developed method can be used to test other atmospheric models.

A METHOD OF EVALUATING ATMOSPHERIC MODELS USING TRACER MEASUREMENTS

Darko Koracin and James Frye
Desert Research Institute, Reno, Nevada

Vlad Isakov
DynTel, Research Triangle Park, North Carolina

1. Introduction

Realistic, three-dimensional atmospheric fields are an essential input for the simulation of transport and dispersion of atmospheric pollutants (e.g., Yamada 1992; Uliasz 1993; Enger and Koracin 1995). The evaluation of wind fields predicted by atmospheric models or obtained from the objective analysis of measurements, however, represents a significant challenge in boundary-layer research. This is especially true for wind fields over complex terrain (e.g., Pielke 1984; Venkatram 1988; Brier 1990; Hanna 1994). Many studies, including a survey by Blumen (1990), have shown that the mean and turbulence properties of airflows in developed topography are usually highly variable in both the spatial and temporal domains. Local circulations are frequent and dominant features, and they usually represent a significant factor in determining the overall dynamics and associated transport and dispersion of atmospheric pollutants in complex terrain.

Many researchers have investigated the evaluation of wind fields through the use of observations (e.g., Clements and Hoard 1989; Whiteman 1982, 1989) and through modeling (Doran and Horst 1983; Yamada and Bunker 1988; Pielke 1984; Enger et al. 1993; Koracin and Enger 1994). Models of various complexities have been commonly evaluated through comparison of trajectories derived from observations of tetroons (Hoecker 1977; Stocker et al. 1990; Yamada 1992) or trajectories estimated from tracer gas measurements (Haagenson et al. 1987, 1990; Kao and Yamada 1988; Klug et al. 1992). Although trajectories determined from observations of the positions of tetroons are generally direct evidence of the wind field structure, tetroons are sometimes subject to uncertainty in vertical position due to radiation, mesoscale pressure perturbations, or high humidity conditions. Trajectories determined from tracer measurements are usually uncertain in mesoscale and regional scale field programs due to insufficient coverage by the tracer measurement sites. Insufficient coverage by tracer receptors prohibits the determination of the exact position of the centerline of the tracer plume; consequently, the estimated tracer trajectories are only an approximate representation of the actual tracer plume. The modeling of back-trajectories leads to uncertain results because it is not possible to account for irreversible turbulent processes. For example, Fast and Berkowicz (1997) found that a back-trajectory analysis of regional-scale modeling results could not identify the surface source regions impacting eastern North America. They attributed this to the fact that, although the forward trajectories of the plume were based on the mean and turbulent wind components, the backward trajectory analysis had no means of treating the irreversible turbulent processes.

Both measured and modeled tracer concentrations are affected by transport and dispersion, further complicating the evaluation of wind fields. Complexity and difficulties in evaluating air

quality dispersion models were discussed by Hanna (1988). He emphasized that review and evaluation of model physical algorithms is usually of greater importance than statistical comparison between the model results and measured data. Hanna (1988) pointed out that data input errors from even a carefully performed field program can induce errors in hourly-average model concentration predictions as large as the predictions themselves. In addition, uncertainty in a model's treatment of turbulence can create an error in predicted concentrations that is as large as the measured concentrations. Yamada et al. (1992) and Klug et al. (1992), among others, presented the approach of indirectly evaluating a meteorological model by comparing simulated tracer concentration with observations. Hanna (1994) pointed out, however, that compensating algorithm errors in integrated atmospheric and dispersion models could cancel out and that this could lead to the incorrect conclusion that the models were performing correctly. Also, in some cases, close agreement between a model and measurements can be spurious or can result from measurements that happen to be located at a point where the model can resolve the main features of the flow. In the latter case, the agreement may be poor at points where measurements are not taken or where the model is not able to resolve local features. These features, however, could be essential in accurately determining the transport and dispersion of atmospheric pollutants. In other cases, the agreement between the model and certain measurements--those made in the most complex topographical region of the domain, for example--can be poor while the main transport in the majority of the domain is still accurately represented. Since a dispersion model generally uses predicted atmospheric fields as input, uncertainty in the atmospheric fields creates and usually amplifies any uncertainty in the results of even a perfect dispersion model.

For these reasons, our main objective was the development of a method of evaluating predicted wind fields using only measured tracer concentrations without introducing dispersion calculations. This is an advantage because any estimates of dispersion involve further assumptions and uncertainties. The use of inert chemical tracers offers an excellent opportunity for the development of a method that uses most probable "true" measurements that can uniquely identify the transport of a pollutant plume. Although the measured tracer concentrations result from both transport and dispersion processes, we can quantitatively describe and determine the wind fields that are able to reproduce the main transport of tracers. It should be emphasized that, in the case of available tracer measurements, this method could be used as a complementary method to the usual qualitative evaluation related to known local circulations and comparison with available meteorological measurements.

2. "Tracer potential" - a method of evaluating predicted wind fields using a cost function

We assume that the atmospheric transport by given wind fields is represented by means of resolved scale trajectories. As a first and obvious step in comparing the wind fields predicted by different atmospheric models, some parameters can be calculated describing the separation between every trajectory segment--as predicted by different models or determined from a measurement network--and a location of maximum measured tracer concentration. This simple approach requires only one location where the maximum concentration is measured. In many cases, however, high concentrations are also measured at other locations; but this spatial information is ignored by using a calculation of the minimum distance between the trajectory and the location with maximum concentration. In addition, this method does not take into account the magnitude of the measured

concentrations. Consequently, the same minimum distances have a different significance when the magnitude of the measured concentrations varies. This analysis led us to develop an approach to comprehensive model evaluation using a cost function. In a spatially variable field of tracer concentrations, it is important how close the predicted plume trajectories are in relation to high concentrations. Therefore, both the minimum distance and magnitude of the measured concentrations are important in evaluation of the predicted wind fields. The cost function approach indicates greater success when the trajectory segment is closer to high concentrations. The total value of the cost function at every point during a period of tracer sampling is defined as a superposition of cost functions at that point with respect to all receptors in the domain. Since the cost function resembles an expression for a physical potential, it has been named the “tracer potential” function. Preliminary results of using the tracer potential method in evaluating atmospheric models were reported by Koracin et al. (1998a, 1998b). The total value of the “tracer potential” (TP) function is:

$$TP(x,y,z) = \sum_{i=1}^n \frac{a c_i^m(x_i,y_i,z_i)}{r_i[(x,y,z),(x_i,y_i,z_i)]^2 r_0} \quad (1)$$

where a is a constant, $c_i^m(x_i,y_i,z_i)$ is the tracer concentration at a receptor i , n is the number of receptors, $r_i[(x,y,z),(x_i,y_i,z_i)]$ is the separation between the end of the trajectory segment (x,y,z) and the particular receptor (x_i,y_i,z_i) , and r_0 is the constant providing a convergent solution when the trajectory passes over the receptor. Since the structure of the cost function is arbitrary, we have selected constants a and r_0 to be unity and have chosen femtoliters per liter [$\text{fl}\mu\text{L}^{-1}$] for tracer concentration and kilometers for distance. According to the present definition, TP is a function of spatial position. However, the spatial structure of the TP is constant during the interval of tracer sampling (in our case, a daily interval). A reference TP (TP_0) can be defined at the source position; TP_0 is constant for the entire sampling period. A change of position along each trajectory will lead to increased or decreased TP. Increased TP indicates that the trajectory is approaching the field of high concentrations and, therefore, performing successfully. While leaving the area of maximum tracer concentrations, TP will decrease and asymptotically approach zero as the distance from receptors becomes larger. Cases with relatively weak concentrations overall will be indicated by a low TP_0 value. In summary, if the trajectory passes through an area of large potential, the result represents close agreement of the trajectory and the actual tracer plume. This method is applicable to different numbers of receptors which is important since the number of receptors with available measurements may vary from day to day, as was the case with our sample data. An increasing ratio between TP and TP_0 indicates that the computed trajectories starting from the source are generally approaching higher concentrations. If the ratio decreases, the trajectories are generally not entering the region of high concentrations.

According to Eq. (1) the TP function is generally three dimensional. In this study, we present a two-dimensional version applied to characteristic levels relevant to surface and elevated transport. In the two-dimensional case, the tracer potential function is:

$$TP(x,y) = \sum_{i=1}^n \frac{a_i c_i''(x_i, y_i)}{r_i[(x,y), (x_i, y_i)] \% r_0} \quad (2)$$

All parameters are the same as in Eq. (1), except that the TP function is calculated at selected vertical planes. Besides the simplicity of a method illustration, we chose to apply the two-dimensional version due to nonavailability of the vertical velocity in some of the wind fields as well as general inaccuracy of the diagnosed and predicted vertical velocity in most of the wind fields.

3. Hypothetical example A - effects of wind direction on reproducing tracer transport

An idealized schematic of the trajectory performance is shown in Fig. 1. Two receptors with high concentrations are indicated in the upper part and two receptors with low concentrations in the lower part of the figure. The success of the simulated or measured and interpolated wind fields will be determined by whether the fields approach receptors with high concentrations in contrast to the receptors with low concentrations. At initiation, all trajectories start from the source. Therefore, the distances to all receptors at the initial time are the same for all trajectories. Since tracer concentrations are daily averages, the initial TP_0 is the same for all trajectories for a given day. If after one time interval the trajectory ends in point A, the new TP will be larger than TP_0 since the distances to receptors with high concentrations become shorter. In contrast, if the trajectory segment after one time interval ends in point B, the new TP will decrease; and this trajectory (Tr_2) will less successfully represent actual wind fields that transported and dispersed tracers than the trajectory (Tr_1).

Our basic motivation to develop a new method of evaluating wind fields is illustrated by Fig. 1. Most of the model evaluation schemes would apply a dispersion model to these wind fields and compare dispersion estimates with measured concentrations. Suppose that the same dispersion model is applied to each of these wind fields. Obviously, if the dispersion model is accurately representing reality and the wind fields are accurate, we would expect good agreement between the model and measurements. However, even if the wind fields are correct, the dispersion model can underestimate or overestimate diffusion, and consequently poorly correlate with measured concentrations at point A. Also, if the model realistically represents diffusion but the wind fields are heading to point B, the agreement will be poor. In all of these cases, it will be unclear whether the problem lies within the dispersion model or estimated wind fields. Moreover, if the wind fields are heading to point B and the dispersion model grossly overestimates dispersion, one might end up with perfect agreement at point A as a result of inaccurate wind fields and wrongly estimated dispersion. As mentioned in the introduction, the problem of evaluating integrated atmospheric and dispersion models has been recognized by Hanna (1994), among others. Hanna indicated that the detailed analysis of model structure and used parameterizations should be the main component in evaluating dispersion model results.

The simplest way of evaluating wind fields is to compare simulated wind parameters with measured ones at available locations. Even with a favorable single-point comparison between the simulated and measured winds at the source and at points A and B, there is no certainty that the transport from the source to either point A or B in complex terrain is well represented by the

simulated wind fields. Tracer experiments with a sufficiently dense network of receptors offer a unique opportunity to detect the occurred transport in most atmospheric conditions. Although a measured tracer concentration is an effect of transport and dispersion, in most of the cases the locations of areas of highest concentrations with respect to the source are evidence of the necessary direction of transport that wind fields need to closely represent. The present method uses all available measured tracer concentrations to credit wind fields that are able to approach areas of high concentrations and discredit wind fields that are not entering the areas of high concentrations. The method does not attempt to judge the ability of wind fields for favorable dispersion estimates and agreement with measurements. This means that the method will not judge whether Tr_1 in our example (Fig. 1) is more successful in representing tracer transport than Tr_3 , but that Tr_1 and Tr_3 are more successful than Tr_2 in representing transport of tracers. The method provides a quantitative measure of success of every tested wind field in representing tracer transport. It should be mainly use to rank the success of different wind fields in representing tracer transport and as a screening method prior to using dispersion models. Consequently, the method can prevent unnecessary changes in dispersion schemes due to inaccurate wind fields. In addition, the most successful wind fields will represent a solid base for necessary improvement of dispersion models.

Since the trajectory can be associated with regions of potential larger than the reference potential (positive performance) as well as with regions of potential smaller than the reference potential (negative performance), we can estimate overall success by integrating the area under the curve of time variation of the potential. The net effect for each trajectory will be the difference between the positive and negative area. Figure 2 illustrates the basic principle of this method. The figure shows the trajectory approaching locations of high concentration during the first two hours and leaving the locations of high concentration during the next three hours. In addition to the net-area effect, the magnitude of the positive area under the TP curve can also be considered a measure of success. In the case of fewer tracer receptors at long distances from the source, test information for tracer potential is reduced. Consequently, the positive area within close range of the source is then the most appropriate test information for evaluation of different wind fields relevant to tracer transport.

Initial TP (TP_0) represents a baseline for determining successful behavior of the predicted and interpolated trajectories. However, TP_0 provides only a relative measure among different wind fields. In order to approximate an absolute measure, we developed a procedure for creating a trajectory which will have a large potential for a given TP field. This procedure is described in section 9a.

4. Hypothetical example B - effects of spatial discretization and magnitude of wind speed on the calculation of the tracer potential

Since the TP function is nonlinear, it is essential to investigate the discretization necessary to fully resolve its spatial properties. The discretization is also related to wind speed since the trajectory parcels with different wind speeds will pass different distances for the same time interval. Let us consider a simple, one-dimensional domain of 100 km with a source at origin and a receptor at a distance of 50 km in the positive X direction. A tracer concentration of $10 \text{ fl} \mu^{-1}$ is assumed at the receptor. Figure 3 shows that the nonlinear tracer potential function can be resolved using small

spatial intervals of 1 km or less. If the calculation is performed at every 10 km, however, the integrated area will be overestimated. In the case of a spatial increment of 30 km, the integrated area will be underestimated. In summary, for a given cost function, the discretization interval for calculation of the tracer potential has to be sufficiently small to resolve the shape of the nonlinear TP function. Figure 4 shows a dependence of calculated net tracer potential area (TPA) on wind speed magnitude. If tracer potential is calculated only at the end of the time interval (e.g., hourly), the tracer potential function will not be properly resolved, resulting in an erroneous estimate of the net tracer potential area. Moreover, this error will be magnified for higher wind speeds, since the spatial discretization will be wider for the same time interval. If the time interval for calculation frequency is reduced (e.g., to approximately 0.01 hr), the erroneous component becomes negligible for the entire interval of wind speeds.

5. Assumptions and uncertainties of the tracer potential method

The TP method assumes that the success of a wind field in representing tracer transport is directly proportional to the magnitude of each tracer concentration and inversely proportional to the distance from the segment of the wind field trajectory to a receptor location. This choice is built into the cost function as a measure of success. The cost function is calculated for each trajectory segment as the superposition of every tracer concentration and the distance from each receptor to that segment. Although we base our analysis on the $1/r$ dependence of the cost function, test results with a cost function with $1/r^n$ dependence are discussed in section 9e. As could be expected, the TP curve exhibited sharper peaks and faster decay around receptors for the exponent greater than one and the opposite behavior for the exponent less than one. In spite of relatively small differences in success between the results from two different formulations of the cost function, the ranking of the success among the wind fields remained the same.

A representation of the atmospheric transport by a given wind field is necessary to calculate the TP function. We have chosen the commonly used spatial trajectories constructed from the gridded wind field data and model results. A better representation of the atmospheric transport in complex terrain, including sub-grid scale effects, would improve the method results. It should be noted that the full and unique representation of sub-grid wind field transport still remains an unresolved issue.

The basic test information for the TP method is measured tracer concentration at all available receptors. The resolution of the tracer measuring stations and wind fields should be determined by the complexity of the terrain. In addition, the placement of the stations must be able to cover the main transport patterns. It is well known that the transport and dispersion of atmospheric pollutants and tracers in developed topography frequently has a complex structure. Complexity of local circulations, turbulence, and stability often induces substantial distortion of the plume. The TP method, as well as other methods of evaluating atmospheric and dispersion models, will always have additional uncertainties since the full spatial and temporal structure of the plume in complex terrain will never be known. A sufficiently dense measurement network, both spatially and temporally, as well as including continuous remote sensing of the three-dimensional plume structure, would definitely improve a basic test of information in the future.

In general, spatially and temporally variable uncertainties in tracer measurements also

influence the accuracy of the TP method. The uncertainties in measuring tracer concentrations are, however, quite small; and the tracers are assumed to be ground truth (see section 7). It should also be emphasized that the uncertainty is the same for all wind fields. The TP method assumes that there is a sufficient number of tracer receptors and that neighboring receptors have relatively small angular differences. Since the receptors close to the source measure generally higher concentrations than the receptors further downwind, the contribution from near-source receptors to calculated TP will be greater. Section 7 discusses available receptor data, specifics of the receptors, their distances from the source, and angular differences between neighboring receptors for each day of the field program. The most appropriate set of days for calculating tracer potential is also suggested. Trajectories start seven hours prior to the beginning of sampling in order to be able to reach receptors at the start of sampling. They are also discontinued before the sampling ends to account for the distance from the source to the nearest receptor. The average measured wind speed (wind profiler and surface station at the source) is used to determine the stop time. Calculation results of the maximum tracer potential curve for points within the entire domain depend on the wind speed measured at the surface station and wind profiler at the source.

In the case of two wind fields with the same directional success (same wind direction), the TP method favors the wind field with lower wind speeds. In other words, a longer residence time for the plume is preferred. This can be explained by the fact that, at the same distance from the source and assuming a constant emission rate, the wind field with low wind speeds will transport a larger mass of pollutants compared to the wind field with higher wind speeds. Considering the principle of conservation of mass of pollutants, this is a valid assumption. However, emphasis on wind fields with low wind speed could have a secondary effect on the TP results compared with a directional effect. In the case that a model significantly underestimates wind speed during the considered period, additional uncertainty can lead to the overestimation of success. The primary objective of the method is to quantitatively credit wind fields that are approaching areas with high tracer concentrations in contrast to wind fields that represent transport toward areas with low tracer concentrations. If tracer concentrations are low in the entire domain, this type of analysis becomes less suitable for evaluation of different wind fields. Low tracer concentrations might correspond, for example, to strong convective mixing or elevated long-range transport. In such cases, however, the initial tracer potential will be small and therefore easily identified for other types of analysis.

It should be noted that in the case of multiple and minimally-separated valleys, the tracer plume can bifurcate. According to the TP method, some trajectories can still be successful without being in the valley with the highest measured tracer concentrations.

As indicated in section 2, we chose to present results from the two-dimensional version of the TP function applied to characteristic levels relevant to the surface and elevated transport of tracers. This version was used since the wind fields considered have differing or no treatment of vertical velocity. In addition, the uncertainty in diagnosing or predicting vertical velocity is generally greater than the uncertainty in diagnosing or predicting horizontal wind components. We also present a method of improving the limitations of the selection of particular vertical levels by estimating the success based on the vertically integrated TP function.

6. Field program

An extensive field program, including meteorological and chemical measurements, was

conducted in the southwestern U.S. in summer 1992 (Pitchford et al. 1997; Green 1998). The main objective of the program was to investigate and identify possible short- and long-term transport and dispersion of atmospheric pollutants from major urban areas and industrial sources to the Grand Canyon and its vicinity. A meteorological network of surface and upper-air stations was established in the region to characterize atmospheric transport. A number of primary and secondary chemical components were measured at most of the meteorological stations. In addition to pollutant measurements, intensive study periods included release of tracers. The main objectives for conducting the tracer measurements as a part of the project Measurements Of Haze And Visibility Experiment (MOHAVE) were to evaluate the performance of source apportionment and receptor models, generate input data for source apportionment models, and characterize atmospheric flows from the release sites to the monitoring locations as a function of meteorological conditions. Perfluorocarbon tracers (PFT) that were used during the field program are inert, non-depositing, and non-toxic chemicals. During most of the winter and summer 1992, the ortho-perfluorodimethylcyclohexane (hereafter oPDCH) tracer was continuously released, at a rate proportional to power production, from the Mohave Power Project (MPP) power plant in Laughlin (35.15E N, 114.59E W), Nevada. Laughlin is located approximately 150 km southwest of the western rim of the Grand Canyon. The Mohave Power Project is a coal-fired power plant with a 150 m tall stack. The area is characterized by a complex topography of river and dry valleys as well as high plateaus (Fig. 5). The power plant is located outside the narrow part of the Colorado River Valley, near the south entrance. During the summer intensive study period, tracer emission was started on 12 July and was performed continuously for the next fifty days. In addition to sparse routine measurements in the area, upper-air and surface meteorological measurements were also conducted during the field program. The upper-air measurements included wind profilers at MPP, Truxton, Overton Beach, and Meadview, as well as airsonde measurements at Cottonwood Cove and Dolan Springs. These upper-air measurements provided data on the vertical structure of winds and atmospheric stability, which were used for model initialization, nudging, and evaluation.

7. Tracer concentrations

Figure 5 shows the positions of tracer receptors relative to a source--MPP--that was operational during the tracer experiment. Using the Briggs formula (Briggs 1975), the estimated mean plume rise is between 200 and 300 m; therefore, the effective plume centerline height is approximately 350-450 m AGL. Inert tracer (oPDCH) was injected into the plume, at a rate proportional to power production, and transported and dispersed within the plume. The full load of oPDCH was approximately 40 mg s^{-1} . Forty-five percent of the oPDCH consisted of an isomer ortho-cis PDCH (hereafter ocPDCH). According to the Project MOHAVE database, the average uncertainty in tracer measurements is only 7%. Taking into consideration the uncertainty in background concentrations as well as tracer measurements with respect to the average values, we used a more conservative average uncertainty of 15% (see below for further explanation). It should be noted that this uncertainty is less for the receptors closer to the source. These receptors in the proximity of the source have higher average concentrations and provide a stronger "signal" for the TP calculation. According to the results of the background study (Green 1998), ambient background concentration of ocPDCH for the period prior to the tracer experiment was $0.52 \text{ [fl}\mu\text{]}^{-1}$ with an uncertainty of $\pm 0.052 \text{ [fl}\mu\text{]}^{-1}$. Green (1998) also reported an uncertainty of $\pm 0.06 \text{ [fl}\mu\text{]}^{-1}$ in

measurements of tracer concentration. Details on tracer measurements can be found in Pitchford et al. (1997); Green (1998); and Kuhns et al. (1998). Table 1 lists available receptor sites and their geographical position. The specifics of tracer receptor position, data availability, and the basic statistics of measured concentrations are shown in Tab. 2. The table shows the uncertainty reported in the MOHAVE database (U1). The second uncertainty (U2) is the ratio between the sum of the uncertainty in the background concentrations and tracer concentrations during the experiment, and the total measured tracer concentrations. The position of all considered receptors within the octants centered at the tracer release source (MPP) is shown in Fig. 6.

Hanna (1994) reviewed studies focused on evaluation of calculated mesoscale and regional-scale trajectories. Most of the studies used either tetroon or tracer measurements to obtain most probable observed trajectories. Hanna concluded that the root-mean-square angular differences among regional observed and calculated trajectories are approximately 20E or larger, and that the root-mean-square differences in distances among the endpoints of observed and calculated trajectories are approximately 100-200 km or larger after one day of travel. Prior to applying the TP method to data and model results from the intensive summer study period, the directional coverage of tracer receptors for each day needs to be examined. Directional coverage is represented by all azimuthal receptor positions with respect to origin at the source. We assume that there is adequate coverage when a) there is at least one operating receptor in each octant, and b) the average angular difference with respect to the source position between the nearest neighboring receptors that were operational is less than 20E. Twenty degrees is approximately half the width of each directional sector.

For each day of the field program, the measure of angular coverage of tracer receptors around a source can be defined as the average difference in angular position between the nearest neighboring receptors that were operational that day. A larger angular coverage is associated with smaller mean angular difference. Reliability of the TP method is greater for a larger number of operational receptors as well as for a larger angular coverage of the receptor positions. When concentrations at receptors are relatively high, a significant amount of test information will be available for the TP method. This test information can be characterized with an initial TP (TP_0). The combination of the number of operational receptors, mean differences in angular position between neighboring receptors, and TP_0 will determine the appropriateness of using the results from the TP calculation for each day. Table 2 also indicates some of the effects of common summertime meteorology in this area on the field of average concentrations. Due to dominant flows from the southwest during the summer, most of the tracers were transported and dispersed to the northeast. This is also evident in Fig. 7 which shows spatial contours of tracer concentrations averaged for the entire period.

For each day of the considered period, Tab. 3 lists the TP_0 , the number of operating receptors in each octant, mean differences in angular position between neighboring receptors, and a flag indicating whether spatial coverage was sufficient with respect to octants. During 40 of 51 days, at least one receptor was in operation in each octant. Mean daily angular separations ranged from 16 to 60E. Days with complete directional coverage were selected and then restricted to cases with mean angular separation of 20E or less. This resulted in a final selection of 38 days with full directional coverage and, at the same time, sufficiently small mean angular separation of receptors. A “plus” sign in Tab. 3 indicates these selected days. From 8 through 13 August, at least two receptors were available in each octant; and the mean angular separation among receptors was 16E. Consequently, this interval was the best period for application of the TP method. Since several

model simulations were also performed for this period, the interval includes the largest number of wind fields available for the TP analysis.

8. Wind fields

Five sets of wind fields characterized by varying complexity of atmospheric information were used for the study:

! Wind profiler data (WP wind fields)

These wind fields were obtained by interpolation and extrapolation of data measured by wind profilers at Mohave Power Project, Meadview, Overton Beach, and Truxton. The profilers were located within a range of 150-200 km around the source (Rodger Ames 1997, personal communication). The measurement data were interpolated and extrapolated for a 300 km by 300 km domain with a resolution of 3 km between grid points. For this analysis, we used available data at 400 m AGL.

! CALMET simulation results (CALMET wind fields)

The second set was derived by Vimont (1997) from the diagnostic atmospheric model CALMET (Scire et al. 1995). CALMET diagnoses gridded wind fields, mixing depth, atmospheric stability classes, some parameters of turbulence transfer, and precipitation. The model uses observations from surface and upper-air weather stations as input. Performance of the model can be enhanced by incorporating data from additional surface, upper-air, and remote sensing measurements. Vimont (1997) performed CALMET simulations for the period of the tracer experiment described in sections 6 and 7. In addition to input data from standard meteorological sources, he used data from wind profilers located at the source (MPP), Meadview (MEAD), and Truxton (TRUX). The model domain encompassed 300 km in the west-east direction and 400 km in the south-north direction with a spatial resolution of 5 km. The model grid consisted of 12 vertical levels from the surface to 3 km AGL. For this study, the wind fields at 20, 200, and 500 m AGL were available for analysis.

! Idealized numerical simulations (EK wind fields)

These wind fields were obtained from the idealized simulations of atmospheric processes in the Colorado River Valley area using a higher-order turbulence closure model (Enger et al. 1993, Koracin and Enger 1994). The model grid covered 300 km by 360 km with 61×41 points. The grid extended telescopically with the highest resolution of 700 m in the center of the domain along the Colorado River Valley. There were 16 vertical points in the simulation from the surface to 7 km AGL. Average afternoon thermal profiles were used as input for all simulations. Instead of day by day simulations, a sequence of simulations was performed with all possible combinations of geostrophic wind speed (three values) and direction (every 10E, i.e., 36 classes). For every hour of the field program, data from the wind profilers at MPP and MEAD were compared with the model results from the same locations. The three-dimensional modeled wind fields that compared most favorably with the wind profiler data were then used as the best dynamical fields for that hour. The sequence of these hourly predicted wind fields was the basis for calculation of hourly trajectories from the source. Notice that the EK wind fields are different from the wind fields obtained by Enger et al. (1993) and Koracin and Enger (1994). They simulated case studies in June 1986 and used measured profiles from the airsonde measurements as input for the model. These two studies

included detailed comparison of the model results with measurements. The EK wind fields were obtained as simplifications of these simulations for average thermal profiles measured in June and July 1986 with a constant geostrophic wind for each day as described above.

! Numerical simulations using Mesoscale Model 5 (MM5) (MM5 wind fields)

The MM5 model was developed by the National Center for Atmospheric Research and Pennsylvania State University (Grell et al. 1995). Since the late 1970s, this model has been used in many studies of regional and mesoscale weather phenomena. Mesoscale Model 5 preprocessing includes an advanced objective analysis of the synoptic data from the global network and provides detailed initial and boundary conditions for simulations. We used a nonhydrostatic version of MM5 with a 3 km resolution. The model domain consisted of 91 x 124 horizontal grid points and 35 vertical levels. The grid was centered at 35.7E N and 114.0E W. In order to include more upper-air measurements in the initialization process, we used an expanded grid of 60 km beyond the boundary of the model grid. Due to high horizontal and vertical resolution as well as a large number of grid points, the model required significant computational effort. Because of this limitation, we simulated atmospheric processes in a specific domain by using the MM5 model for a selected episode from 7 through 14 August 1992.

! Numerical simulations using the Higher Order Turbulence Model for Atmospheric Circulation (HOTMAC) (HOTMAC wind fields)

HOTMAC is a higher-order closure mesoscale and regional scale model that has been used in a variety of atmospheric and dispersion studies. The basic structure of the model algorithm was described by Yamada and Bunker (1988, 1989), and a comprehensive model evaluation was provided by Yamada and Henmi (1994). Lu and Yamada (1998) performed a numerical simulation for the Colorado River Valley area using the HOTMAC model for the period 6 to 16 August 1992. The model grid consisted of 93 x 64 horizontal grid points and 26 vertical grid points. Since the horizontal resolution was 4 km, the model domain covered an area of 372 km in the east-west direction and 256 km in the north-south direction. Upper-air observations from Cottonwood Cove, Dolan Springs, and Page as well as wind profiler data from Meadview, MPP, and Truxton were used for model nudging. The simulation covers a time period from 0400 LST on 5 August through 1000 LST on 17 August 1992.

9. Intercomparison among wind fields using the TP method

The TP method was applied to the wind fields described in the previous section for the time period covered by the tracer experiment. Details of the calculation procedure are given below.

a. Description of the calculation algorithm

The procedure used to calculate tracer potential for wind fields used in the present study is described in this section. The method requires certain conditions to be applicable to the data for proper evaluation of the wind fields:

- ! Discretization interval must be sufficiently small.
- ! Calculations should be made on the same domain for all wind fields.
- ! Calculation periods must be the same for all wind fields.

In the present study, the wind fields used were generated by different models which used different domains. Therefore, our calculation was made on a common domain, which was formed from the intersection of the individual model domains. This common domain was a 240 km square, with the southwest corner located at 34.7115EN, -115.4768EW.

Since the sampling period for tracers was 24 hours, from 0700 LST to 0700 LST the next day, a 28-hour calculation period was used in the present study, starting at midnight local time and ending at 0400 LST the next day. This three-hour difference between the end of the study period and the end of the sampling period allowed for the fact that the last trajectory created needs some time to reach the receptor nearest to the source, and so must start some time earlier than the end of the calculation period.

The first step in calculating tracer potentials is to generate a set of trajectories using different wind fields. Beginning at 0000 LST, a trajectory was generated at each hour. This trajectory propagated according to the wind fields until it either left the domain or the study period ended. Twenty eight trajectories were generated for each day. Since winds are highly spatially and temporally variable in complex terrain, it is valuable to estimate the level of that variability within each grid cell through which a trajectory is passing. Confidence in the estimation of the trajectory increases as variability decreases. One of the possible measures of variability (*var*) is the standard deviation of the wind component as normalized by the mean value within the grid points that are bordering the grid cell (John Irwin 1998, personal communication):

$$var = \left(\frac{s_u}{u} \% \frac{s_v}{v} \right) \quad (3)$$

A low value of *var* for a given wind field does not necessarily mean that the wind field is performing well. A large *var* can be realistic due to the complexity of the airflows in complex terrain. In such a case, however, the large *var* means that there could be more uncertainty in the calculation of trajectories. As can be expected, the variability is greatest near the surface; for wind fields with equidistant horizontal resolution (CALMET, HOTMAC, and MM5), *var* ranges from 30 to 48%. The variability at 1500 m is much less, ranging from 3 to 29%.

From the set of trajectories described above and the measured tracer concentrations at a series of measuring stations, a set of tracer potential curves was generated. We used a suitably small time interval of 60 seconds to calculate tracer potential along each trajectory, obtaining a tracer potential curve for each. Integrated tracer potential area was then calculated as the area between the tracer potential curve and the reference tracer potential line (TP₀), using the same integration time step. Finally, the area under all 28 potential curves was summed and the average over the total number of hours taken.

In order to obtain a reference value to scale all TP areas for different wind fields, we constructed a trajectory having a "maximum" tracer potential. Note that since we had only limited knowledge of actual winds, this trajectory could only be roughly estimated. This procedure enabled us to compare TPs from different wind fields that were scaled by the maximum potential as well as to determine the fractional success of each wind field with respect to an estimated maximum. At each hour of the study period, wind profiler data of wind speed and wind direction at the source were used. Then, using a suitably small time step of 60 seconds, a hypothetical line was constructed from the source propagating to points at a 1E interval along an arc of 140E centered on the wind profiler

direction. The point with the largest potential was selected as the new current position and the process repeated for the full hour, at which time a new value for wind speed and direction was taken.

The restriction to an arc around the wind profiler direction was a compromise between two conflicting factors. The measured value, of course, is accurate only where and when it is measured. Therefore, as the line propagates further from the starting point, the direction is less likely to correspond to the actual wind direction. If the algorithm is allowed to ignore wind direction entirely and search for a maximum around an arc greater than 180E, however, the generated line seeks the nearest point of high concentration, then oscillates around that point.

b. Success of wind fields as inferred from the net tracer potential area

This method is mainly appropriate for cases with sufficient spatial coverage of near and far receptors around the source.

A time series of the initial TP (TP_0) is shown in Fig. 8. Initial TP was low during the first part of the study period (Julian days 195-214) as well as at the end of the period (Julian days 229-238 and 240-244). A time series of the net area under the TP curve, as estimated for all considered wind fields is shown in Fig. 9. For the days with insufficient receptor coverage of octants, the line is shown without symbols. Tracer potential was calculated as the average of the net tracer potential area of all individual trajectories for a particular sampling day.

There is general agreement among the TP values calculated from different wind fields. Periods with increased TP as captured by more than one set of wind fields occurred in the second part of the period. In these cases, the wind fields were generally able to approach high measured concentrations. In contrast, there were periods when most of the wind fields were not able to create positive net-area potential (e.g., Julian day 219). These periods were usually associated with variable weather phenomena that could not be resolved either by the models or relatively coarse measurements. In some instances, a large TP corresponds to a situation in which high tracer concentrations were measured near the source, causing TP to decrease toward negative values relatively soon after leaving the near-source area.

It is interesting to note that in some cases increased tracer potential did not necessarily represent significant success since the maximum potential could be much larger than the potential associated with modeled wind fields (e.g., Julian days 226 and 227). In some other cases, when the maximum TP is small, wind fields can be regarded as successful even though the magnitude of the TP is relatively small. In addition, actual plume centerline might have been significantly different than the assumed value (350-450 m AGL). The “absolute” success (s_{an}) in this case is defined as:

$$s_{an} = \frac{TP_{net}}{TP_{maxn}} \quad (4)$$

where TP_{net} is the net tracer potential area, and TP_{maxn} is the maximum net tracer potential area. Points where the formula yields a negative value are considered zeroes.

An analysis of the wind field success rates for the most probable plume effective height indicated that the inferred success varied considerably from day to day for all the wind fields. CALMET generally had the greatest success; the formula yielded only positive values for TP area during the entire period. During 23 out of 40 days, CALMET had success rates greater than 10%,

with a maximum of 22%. EK had relatively low success, and negative TP area on 11 of 51 days. Maximum success was 12%. HOTMAC showed a negative TP area on two out of ten days. The maximum success was 17%; and during a four-day period, the maximum was greater than 10%. MM5 showed a negative TP area only on one day and on two of eight days had success greater than 10%. The WP fields had the largest maximum (37%), but with variable daily success and negative TP area on eight out of thirty-nine days.

c. Success of wind fields as inferred from the positive tracer potential area

This method is mainly appropriate in cases when the emphasis is on the performance of the near-source receptors.

A positive area under the TP curve was a better indicator of success when the maximum tracer concentrations were measured near the source and the negative area was created soon after leaving the high tracer concentrations. The success in this case (s_{ap}) is defined as:

$$s_{ap} = \frac{TP_{pos}}{TP_{maxp}} \quad (5)$$

where TP_{pos} is the positive tracer potential area, and TP_{maxp} is the maximum positive tracer potential area.

Figure 10 shows a time series of the positive tracer potential area at the most probable effective plume height for July and August 1992. Both Figs. 9 and 10 indicate several important features. None of the wind fields show superior performance for the entire period. According to the present method, interpolated and extrapolated data from wind profiler measurements (WP) showed the greatest success only in certain episodes (Julian days 205-207 and 226-232) and could not represent the most probable tracer transport during Julian days 208-209, 214-215, and 223-225. Numerical modeling (EK) using only summer average thermal profiles as well as temporarily and spatially constant geostrophic wind during each day provided quite reasonable success, mainly during Julian days 215-225. The diagnostic model using wind profiler data (CALMET) provided very good results during the considered period and generally represented an improvement compared to the use of measurements only (WP). Average success for all wind fields was from 6 to 12%, and the median was from 4 to 12%. Wind fields derived from the CALMET model had a significant number of days with success rates between 10 and 22% and a relatively high mean success rate. Idealized numerical simulation (EK) wind fields had success rates between 0 and 23% with a relatively low average value. For the limited available period of 10 days, HOTMAC showed daily success rates ranging from 0.3 to 17%. For the eight available days, the MM5 success rate ranged from 4 to 20%. The wind profiler fields showed quite variable success rates, ranging from 0 to 37% during the available period. Although the maximum is quite high, the average success of the WP fields is lower than that obtained from the CALMET, HOTMAC, and MM5 models. Incorporation of measurements into a diagnostic model (CALMET) appears to significantly improve the success rates. HOTMAC wind fields nudged with measurements yielded success rates similar to MM5 without any additional nudging.

d. *Success of wind fields as inferred from the vertically-integrated positive tracer potential area*

This method can be used when wind fields are diagnosed or predicted at vertical levels representative of near-surface and elevated transport.

A significant portion of the plume could have remained near the ground and been transported toward receptors by near-surface winds. Since near-surface winds are highly variable in complex terrain, it is useful to calculate the TP for predicted or estimated winds from the surface to the assumed average plume effective height. The information on winds at various levels was available from CALMET, EK, HOTMAC, and MM5 wind fields.

Since there is no certainty that the wind fields need to maximize TP for all levels, the height-integrated value of the positive TP area might be calculated. The integrated value of the positive TP area for at least several vertical levels will represent the overall success of a particular wind field. This could be another measure of success in addition to the basic approach we have suggested involving calculation of TP for the most probable effective plume height. In this case, the success (s_{ai}) is defined as:

$$s_{ai} = \frac{TP_{int}}{TP_{maxi}} \quad (6)$$

where TP_{int} is the vertically-integrated positive tracer potential area, and TP_{maxi} is the maximum vertically-integrated positive tracer potential area.

Several vertical levels between the surface and the effective plume height are available from CALMET, EK, HOTMAC, and MM5 wind fields. We selected three vertical levels: a) first model level near the surface (10-20 m AGL); b) level located approximately in the middle between the surface and the plume effective height (approximately 150-250 m); and c) nearest level to the effective plume height (350-450 m AGL). Maximum TP was calculated for each level. The magnitude of the surface wind speed at the source was used for the maximum TP at the surface level, while the wind profiler winds were used for calculation of the maximum TP at two upper levels. Since the wind speeds were generally lower near the surface, the TP and maximum TP were generally larger. The total maximum TP was then calculated as a sum of all three maxima. Tracer potential for each wind field and level was calculated in the same way as in section 9c. The total TP for each wind field was then calculated as the sum of all three levels. The success of a particular wind field is represented by the ratio of the total TP to the total maximum TP. Figure 11 shows a time series of the positive integrated TP, and Tab. 4 lists the corresponding percentages of success with respect to the integrated maximum positive potential area. Wind fields simulated by CALMET, HOTMAC, and MM5 showed similar success, while the EK wind fields showed lower values for four days at the end of the period. It is important to notice that although the estimate of success was different from that obtained by using only the most probable effective plume height, the overall success remained quite similar. For the limited number of available days, numerical models nudged with some of the measurements (HOTMAC) yielded somewhat better results than the CALMET, EK, and MM5 fields. HOTMAC created a success rate between 4 and 28% with three days above 20%. Fields obtained with CALMET, EK, and MM5 showed similar success from day to day in a range between 3 and 16%.

In order to examine the differences between the two-dimensional and three-dimensional

representations of tracer transport, we have tested an area enclosing estimated trajectories at the surface, source height, and the most probable effective plume height levels with respect to an area of surface concentration greater than $0.1 \text{ fl} \mu^{-1}$. The concentrations were predicted by the Lagrangian random particle model (Koracin et al. 1998c) using the three-dimensional MM5 wind fields as input. Following Klug et al. (1992), we compared the trajectory-enclosed area with the surface area of simulated concentrations. Simulated and trajectory-enclosed areas are denoted as S and T , respectively. The level of agreement is then defined following Klug et al. (1992) for the Figure of Merit in Space (FMS):

$$FMS = \frac{S \cap T}{S \cup T}$$

where the term in the numerator is the cross section between the area of simulated concentrations and the trajectory-enclosed area, while the term in the denominator is the union of both the area of simulated concentrations and the trajectory-enclosed areas. The FMS ranges from 0 (no agreement) to 1 (perfect agreement). We calculated the FMS for the period 6 through 9 August 1992 for three levels. The FMS was relatively high for this limited sample ranging from 0.38 to 0.67, 0.35 to 0.50, and 0.32 to 0.50 for the surface, source height, and the most probable plume effective height, respectively. A possible reason for this relatively good comparison is that there was generally sufficient vertical mixing and small vertical directional shear.

e. Sensitivity of wind field success ranking on a variation of the cost function expression

Our initial choice of the inverse-distance dependence in a cost function was for both simplicity and analogy to physical potential. We have, however, examined other functional relationships, one of which is the inverse square-root dependence in a cost function (Eq. 1). This choice widens the TP function around a receptor, creating generally larger TP along individual trajectories, but also increases the TP. A scatter plot of success as determined from the average value of the positive TP area calculated using the two functions is shown in Fig. 12. The consistency of the overall success ranking is quite obvious. For most of the days available for comparison, CALMET generally created a higher success rate for both formulations of the cost function. Notice that the correlation coefficient between the success obtained with CALMET and EK is relatively high and generally the same for both formulations. If the different formulations would result in success on opposite sides of the 1:1 line, this type of analysis would be inconclusive.

Figure 13 shows a ten-day time series of success for inverse linear and inverse square root formulations. The results were quite similar for square-root and inverse linear formulations, and the relative distribution and success ranking were the same. In summary, the success ranking among different wind fields remained generally the same for different formulations of the cost function.

10. Summary and conclusions

We have developed a method that uses tracer measurements to evaluate wind fields produced by either models or by objective analysis. The most important use of this method is to select the

wind fields that are best able to represent tracer transport. The method can be used as a screening tool to provide the most successful wind fields to dispersion modelers. This application yields a solid base for necessary improvement of dispersion models and prevents erroneous modifications of the models due to inaccurate wind fields.

The method uses a cost function to measure the success of the wind fields in reproducing the transport of tracers. The cost function can be considered to be a “tracer potential” because it is analogous to a physical potential. The relative success of each trajectory is proportional to the difference between the tracer potential and a reference tracer potential. The reference tracer potential is determined for each day by the location of the source and receptors and by the measured daily concentrations at all receptors. A high potential relative to the reference potential along a trajectory indicates a good performance of the wind fields and vice versa. The relative success of a wind field is represented by the net, positive, and the vertically-integrated areas under the tracer potential curve. A trajectory with a maximum tracer potential can be constructed to estimate the absolute success of different wind fields in reproducing the transport of tracers. The integrated area under the tracer potential curve of this trajectory is used to normalize the positive and net areas obtained from particular wind fields. The tracer potential area, vertically integrated from several levels, appears to be a good indicator of the success of a particular wind field. The method is not very sensitive to the exact mathematical form of the tracer potential. For example, a tracer potential with an inverse square-root distance dependence in the cost function yielded the same success ranking of wind fields as a tracer potential with an inverse linear distance dependence.

We used the tracer potential method to determine to what extent and to what degree of confidence simulated wind fields (compared to wind fields derived from measurements) can be applied to drive the transport of atmospheric pollutants in complex terrain. Our data was provided by a field program that was conducted in the southwest U.S. during summer 1992. Success, as expressed in terms of the ratio between the calculated net-area potential and the calculated maximum net-area potential for one week, indicated substantial variation from day to day. According to our tracer potential method, the daily success of the wind fields that we evaluated were quite variable, ranging from 0 to 37%. Average success rates (depending on the temporal length of the available wind fields) were between 4 and 15%. Interpolated and extrapolated data from four wind profilers located in the field program area provided good but variable overall success in describing the transport of tracers. A diagnostic model which incorporated wind profiler measurements (CALMET) was quite successful in describing the tracer transport when compared to measurements only (WP fields) or compared to prognostic models. Day-by-day numerical simulations with the high-resolution mesoscale model (HOTMAC) achieved success similar to CALMET and MM5 in its ability to represent the transport of tracers at the most probable effective plume height. The HOTMAC simulation, however, which was nudged by balloon and wind profiler data, was more successful than the other wind fields in representing the vertically integrated success rate of tracer transport. Part of the success could be attributed to low simulated wind speeds near the surface. In summary, we found that simple interpolation and extrapolation of the data measured by three wind profilers in a complex-terrain domain can only partly describe tracer transport. Idealized and simplified simulations can be used to describe the overall tracer transport and some of the episodes where measurements are not available. A diagnostic model incorporating measurements appeared to be a very successful and computationally efficient tool for creating wind fields that produce a reasonable approximation of tracer transport. The high-resolution prognostic models were quite

successful in describing tracer transport but were limited to relatively short time intervals of 8 and 11 days, respectively, due to high computational demand. Incorporation of measurements and model nudging appeared to improve the success of the wind fields in describing tracer transport.

The tracer potential method can also be used to determine the conditions where relatively coarse measurements can be used to successfully represent the transport of pollutants. In some periods, the wind fields--based on interpolation and extrapolation of measurements--appeared to be unsuccessful in describing the transport of tracers. This indicates that certain weather patterns in complex terrain can be reproduced only with increased spatial resolution of measurements. The periods when the wind fields were not able to capture some weather phenomena (and their variability) could be used for detailed analysis leading to the refinement of existing atmospheric models or the development of new models. In some cases, the "unsuccessful" wind fields could be attributed to elevated plume transport. Time periods when most of the wind fields correlate with increased tracer potential can be identified. These periods can then be used for dispersion calculations.

Our approach and this data from the 1992 field program can be used for the evaluation of additional atmospheric models prior to applying their results to the transport and dispersion of atmospheric pollutants because the data are publicly available.

Future work will focus on estimating three-dimensional trajectories and minimizing the uncertainty in their calculation. Additional remote sensing and aircraft measurements are needed during tracer experiments to shed more light on the transport and dispersion of atmospheric pollutants in complex terrain, as well as to further evaluate this method.

Acknowledgments. This study was supported by Southern California Edison, Los Angeles, CA, EPRI, Palo Alto, CA, and partially by the Department of Defense, Office of Naval Research, Marine Meteorology and Atmospheric Effects, grants N00014-96-1-0980 and N00014-96-1-1235. One of the authors (Vlad Isakov) performed most of the work while he was affiliated with the Desert Research Institute (DRI), Reno, Nevada, U.S. The authors would like to thank Mr. John Vimont and Mr. Rodger Ames of the National Park Service, Colorado and Dr. Ted Yamada of Yamada Science and Art Corp., Santa Fe, New Mexico for kindly supplying the wind field data. Discussions with the Project MOHAVE Steering Committee have helped to improve the study. Valuable comments were provided by Dr. Warren White of Washington University, St. Louis, Missouri. The authors would like to thank Dr. Marc Pitchford of NOAA, Las Vegas, Nevada; Dr. Rob Farber of Southern California Edison, Los Angeles, California; Dr. Leif Enger of the University of Uppsala, Sweden; and Dr. John Watson and Dr. Yangang Liu (DRI) for encouragement, valuable comments, and suggestions. We are very grateful to Mr. John Irwin of EPA (Research Triangle Park, North Carolina) for in-depth comments and suggestions that significantly improved the manuscript. The authors are indebted to Dr. William Stockwell (DRI) for providing very valuable scientific and editorial comments leading to significantly better presentation of our method and results. Discussion with Dr. Hampden Kuhns of DRI, Las Vegas, in analysis of tracer data is greatly appreciated. The authors would also like to thank Mr. Travis McCord (DRI) for technical preparation of the manuscript, and Mr. Roger Kreidberg (DRI) for editorial assistance.

REFERENCES

- Blumen, W., ed., 1990: *Atmospheric Processes over Complex Terrain*. Meteorological Monographs, Vol. 23, No. 45, American Meteorological Society, 323 pp.
- Brier, G. W., 1990: A historical and personal perspective of model evaluation in meteorology. *Bull. Amer. Meteor. Soc.*, **71**, 349-351.
- Briggs, G., 1975: Plume rise predictions. ATDL No. 75/15, Atmos. Turb. and Diff. Lab., NOAA Environ. Res. Lab., Oak Ridge, TN, 53 pp.
- Clements, W. E., and D. E. Hoard, 1989: Mean structure of the nocturnal drainage flow in a deep valley. *J. Appl. Meteor.*, **28**, 457-462.
- Doran, J. C., and T. W. Horst, 1983: Observations and models of simple nocturnal slope flows. *J. Atmos. Sci.*, **40**, 708-717.
- Enger, L., D. Koracin, and X. Yang, 1993: A numerical study of boundary layer dynamics in a mountain valley. Part 1. Model validation and sensitivity experiments. *Bound-Layer Met.*, **66**, 357-394.
- Enger, L., and D. Koracin, 1995: Simulations of dispersion in complex terrain using a higher-order closure model. *Atmos. Environ.*, **29**, 2449-2466.
- Green, M. C., 1999: The Project MOHAVE tracer study: Study design, data quality, and overview of results. *Atmos. Environ.* (in press).
- Grell, G. A., J. Dudhia, and D. R. Stauffer, 1995: A Description of the Fifth-Generation Penn State/NCAR Mesoscale Model (MM5), NCAR Techn. Note TN-398, 122 pp.
- Haagenson, P. L., Y.-H. Kuo, M. Skumanich, and N. L. Seaman, 1987: Tracer verification of trajectory models. *J. Climate Appl. Meteor.*, **26**, 410-426.
- Haagenson, P. L., K. Gao, and Y.-H. Kuo, 1990: Evaluation of meteorological analyses, simulations, and long-range transport calculations using ANATEX surface tracer data. *J. Appl. Meteor.*, **29**, 1268-1283.
- Hanna, S. R., 1988: Air quality model evaluation and uncertainty. *J. Air Pollut. Control Assoc.*, **38**, 406-412.
- Hanna, S. R., 1994: Mesoscale meteorological model evaluation techniques with emphasis on needs of air quality models. *Mesoscale Modeling of the Atmosphere*, R. A. Pielke and R. P. Pearce, Eds., Meteorological Monographs, Vol. 25, No. 47, American Meteorological Society, 47-58.

- Hoecker, W. H., 1977: Accuracy of various techniques for estimating boundary-layer trajectories. *J. Appl. Meteor.*, **16**, 374-383.
- Kao, C. Y. J., and T. Yamada, 1988: Use of the CAPTEX data for evaluations of a long-range transport numerical technique. *Mon. Wea. Rev.*, **116**, 293-306.
- Klug, W., G. Graziani, G. Grippa, D. Pierce, and C. Tassone, 1992: Evaluation of long term atmospheric transport models using environmental radioactivity data from Chernobyl accident. *The ATMES report*, Elsevier, 366 pp.
- Koracin, D., and L. Enger, 1994: A numerical study of boundary layer dynamics in a mountain valley. Part 2. Observed and simulated characteristics of atmospheric stability and local flows. *Bound.-Layer Met.*, **69**, 249-283.
- Koracin, D., V. Isakov and J. Frye, 1998a: A method of evaluation of atmospheric and dispersion models by using tracer measurements. *Proc. Tenth Joint Conference on the Applications of Air Pollution Meteorology with the AWMA*, Jan. 11-16, 1998, Phoenix, AZ, 11-16.
- Koracin, D., V. Isakov and J. Frye, 1998b: A method of evaluating atmospheric models by using tracer measurements. *Proc. Fifth International Conference on Harmonisation within Atmospheric Dispersion Modeling for Regulatory Purposes*, May 18-21, 1998, Rhodes, Greece, 79-86.
- Koracin, D., V. Isakov and J. Frye, 1998c: A Lagrangian particle dispersion model (LAP) applied to transport and dispersion of chemical tracers in complex terrain. *Proc. Tenth Joint Conference on the Applications of Air Pollution Meteorology with the AWMA*, Jan. 11-16, 1998, Phoenix, AZ, 227-230.
- Kuhns, H., M. Green, M. Pitchford, L. Vasconcelos, W. White, and V. Mirabella, 1999: Attribution of particulate sulfur in the Grand Canyon to specific point sources using tracer-aerosol gradient interpretive technique (TAGIT). *J. Air Waste Manag. Ass.*(in press).
- Lu, X., and T. Yamada, 1998: Numerical simulation of airflows and tracer transport in an arid western mountain area. *Proc. Tenth Joint Conference on the Applications of Air Pollution Meteorology with the AWMA*, Jan. 11-16, 1998, Phoenix, AZ, 364-368.
- Pielke, R. A., 1984: *Mesoscale Meteorological Modeling*. Academic Press, 612 pp.
- Pitchford, M., M.C. Green, and R. J. Farber, 1997: Characterization of regional transport and dispersion using Project MOHAVE tracer data. *Proc. Visual Air Quality Conference*, Sept. 9-12, 1997. Bartlett, NH, 181-200.
- Scire, J. S., E. M. Insley, R. J. Yamartino, and M. E. Fernau, 1995: User's guide for the CALMET Meteorological Model. USDA Forest Service Tech. Rep. 1406-01, Cadillac, MI, by Earth

Tech, Concord, MA.

- Stocker, R. A., R. A. Pielke, A. J. Verdon, and J. T. Snow, 1990: Characteristics of plume releases as depicted by balloon launchings and model simulations. *J. Appl. Meteor.*, **29**, 53-62.
- Uliasz, M., 1993: The atmospheric mesoscale dispersion modeling system. *J. Appl. Meteor.*, **32**, 139-149.
- Venkatram, A., 1988: Model evaluation. *Lectures on Air Pollution Modeling*, Amer. Meteor. Soc., 308-321.
- Vimont, J., 1997: Evaluation of the CALMET/CALPUFF modeling system using Project MOHAVE tracer and implications for sulfate contributions. *Proc. Visual Air Quality Conference*, Sept. 9-12, 1997. Bartlett, NH, 436-446.
- Whiteman, C. D., 1982: Breakup of temperature inversions in deep mountain valleys. Part I: Observations. *J. Appl. Meteorol.*, **21**, 270-289.
- Whiteman, C. D., 1989: Morning transition tracer experiments in a deep narrow valley. *J. Appl. Meteorol.*, **28**, 620-635.
- Yamada T., 1992: A numerical simulation of airflows and SO₂ concentration distributions in an arid south-western valley. *Atmos. Environ.*, **26A**, 1771-1781.
- Yamada, T., and S. Bunker, 1988: Development of a nested grid, second-moment turbulence closure model and application to the 1982 ASCOT Brush Creek data simulation. *J. Appl. Meteor.*, **27**, 562-578.
- Yamada, T., and S. Bunker, 1989: A numerical model study of nocturnal drainage flows with strong wind and temperature gradients. *J. Appl. Meteor.*, **28**, 545-554.
- Yamada, T., S. Bunker, and S. Moss, 1992: Numerical simulation of atmospheric transport and diffusion over coastal complex terrain. *J. Appl. Meteor.*, **31**, 565-578.
- Yamada, T., and T. Henmi, 1994: HOTMAC: Model performance evaluation by using project WIND Phase I and II Data. *Mesoscale Modeling of the Atmosphere*, R. A. Pielke and R. P. Pearce, Eds., Meteorological Monographs, Vol. 25, No. 47, American Meteorological Society, 123-135.

Figure Captions

- Fig. 1. Illustration of the tracer potential (TP) method for two trajectories originating from a source. Tracer potential of Trajectory 1 is increasing along a path approaching high tracer concentrations (c_1 and c_2); TP of Trajectory 2 is decreasing along a path approaching low tracer concentrations (c_3 and c_4) (see text).
- Fig. 2. Illustration of the integrated net area under the TP curve as a difference between a positive (“successful effect”) and a negative (“unsuccessful effect”) area. TP_0 is a reference value.
- Fig. 3. Tracer potential function versus downwind distance from the source located at origin. A receptor is located at 50 km from the source, and the domain extends to 100 km. The discretization spatial increments of resolving the function are: 1 km (dotted), 10 km (dashed), and 30 km (solid line).
- Fig. 4. Net tracer potential area estimated for the hypothetical example B (see text and Fig. 3) as a function of the range of wind speeds. The discretization time increments of resolving the function are 1 (o), 0.5 (x), 0.1 (+), and 0.01 hr (*).
- Fig. 5. Topography of the Colorado River Valley area centered at (35.7E N, 114.0E W) with indicated source and receptor locations. Contour interval of the surface elevation is equal to 100 m.
- Fig. 6. Position of the tracer receptors (see Tab. 2) in octants centered at the tracer release source (MPP).
- Fig. 7. Contours of the tracer concentration as averaged for the period from 5 July through 5 September 1992. Contour interval of the tracer concentrations is $0.25 \text{ [fl}\mu\text{]}^{-1}$, and a background contour interval of surface elevation is 200 m.
- Fig. 8. Time series of the initial tracer potential for the studied area in summer 1992.
- Fig. 9. Time series of the net tracer potential area for all available wind fields for each day.
- Fig. 10. Time series of the positive tracer potential area for wind fields as simulated by CALMET, EK, and interpolated from WP data (solid lines with indicated symbols) with estimated maximum net tracer potential area (dashed line) for each day.
- Fig. 11. Time series of the vertically-integrated positive tracer potential area for all available wind fields (solid lines with indicated symbols) with estimated maximum vertically-integrated positive tracer potential area (dashed line) for each day.
- Fig. 12. Scatter plot of the positive tracer potential area for CALMET and EK wind fields using inverse distance cost function (o) and inverse square-root distance cost function

(+). Correlation coefficients are 0.77 and 0.76, respectively, and the number of points is 51 in each case.

Fig. 13

Time series of the positive tracer potential area for all available wind fields using different cost functions: inverse distance (a) and inverse square-root distance (b).

Table Captions

- Table 1. List of tracer receptor sites and their geographical position.
- Table 2. List of receptors with specifics of their distance and angular position with respect to the tracer release source (MPP), and basic statistics of the tracer concentrations (C) measured during the field program.
- Table 3. Number of operational receptors for each octant, mean differences in their angular position, and initial TP for each day of the field program (see text). The flag value of 0 means that at least one octant did not have an operational receptor; 1 means there was at least one operational receptor in each octant; and 2 means there were two or more operational receptors in each octant. The days selected for analysis are indicated in the last column.
- Table 4. Daily percentages of success of each wind field in representing the tracer transport by using the vertically-integrated positive tracer potential area with respect to a maximum integrated positive tracer potential area (see text).

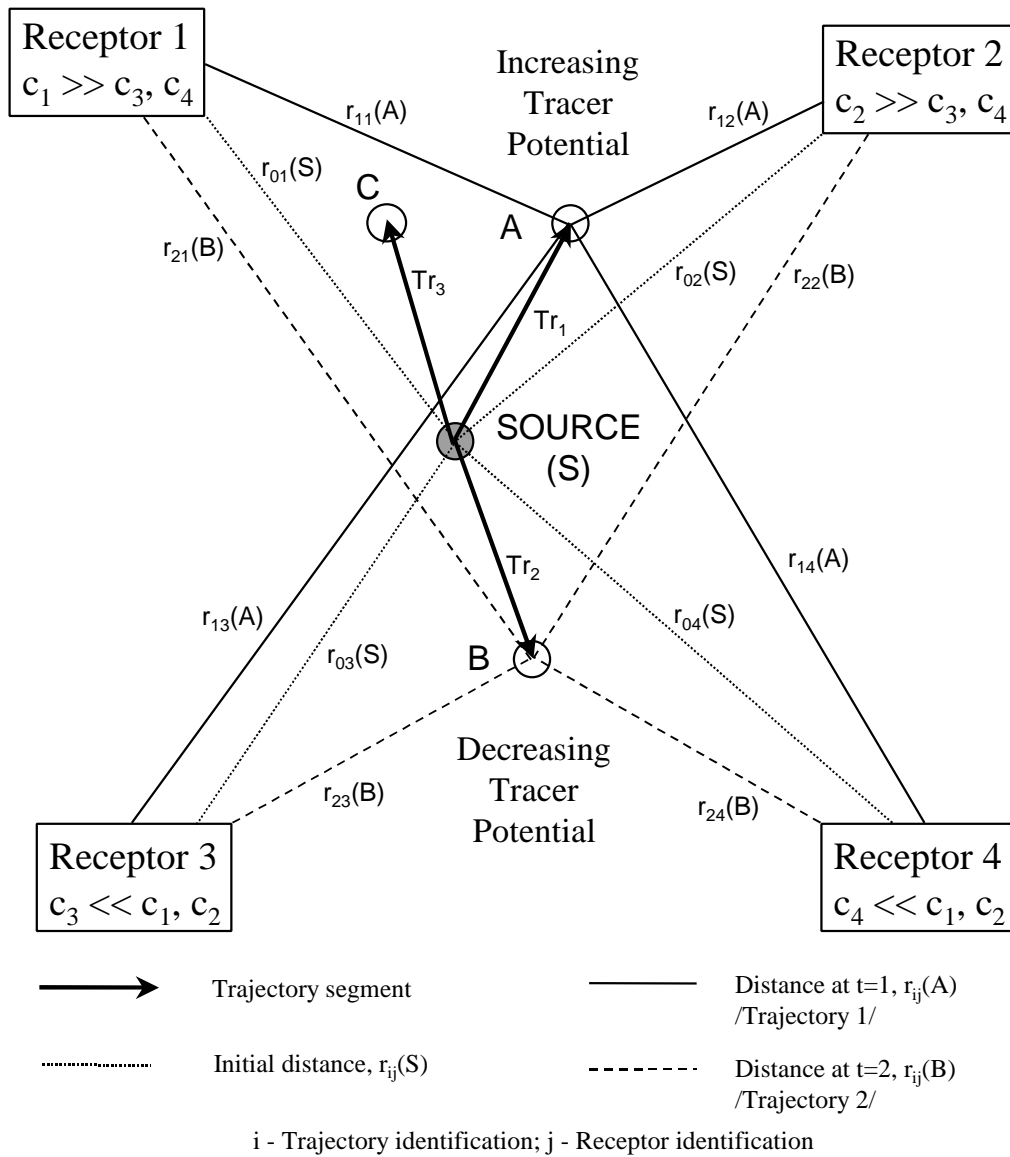


Figure 1. Illustration of the tracer potential (TP) method for two trajectories originating from a source. TP of trajectory 1 is increasing along a path approaching high tracer concentrations (c_1 and c_2); TP of trajectory 2 is decreasing along a path approaching low tracer concentrations (c_3 and c_4) (see text).

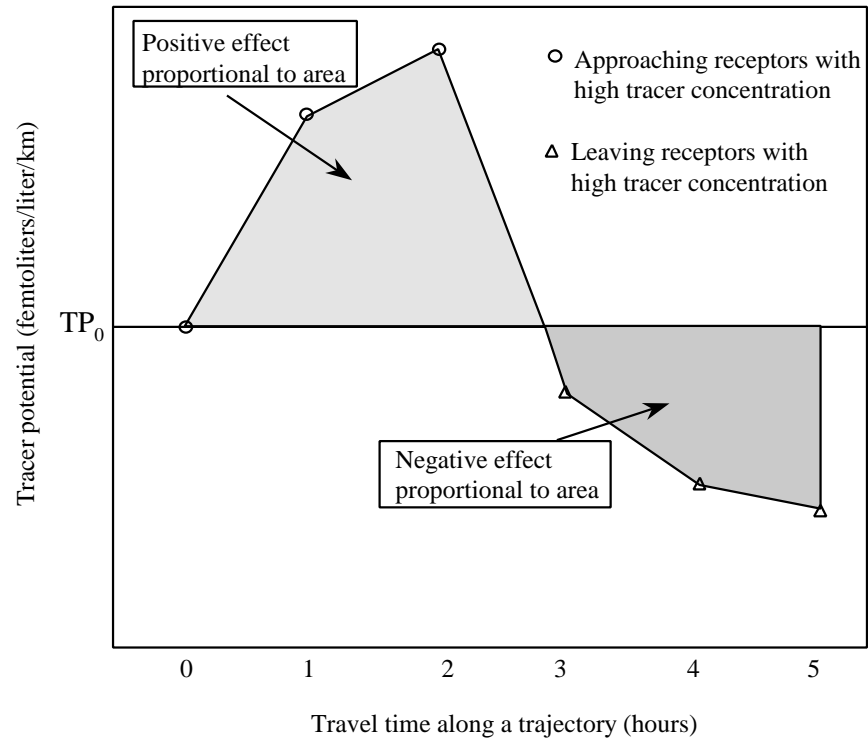


Figure 2. Illustration of the integrated net area under the TP curve as the difference between a positive (“successful effect”) and a negative (“unsuccessful effect”) area. TP₀ is a reference value.

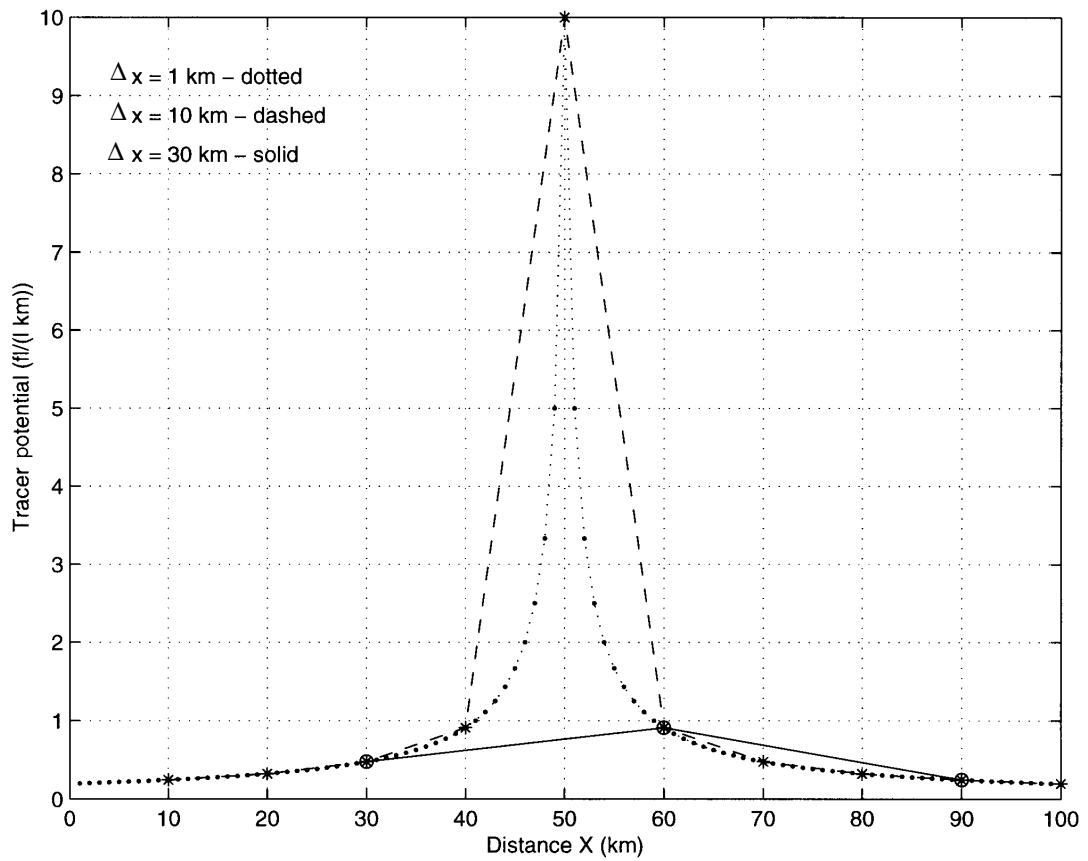


Figure 3. Tracer potential function versus downwind distance from the source located at origin. A receptor is located at 50 km from the source and the domain extends to 100 km. The discretization spatial increments for resolving the function are: 1 (dotted), 10 (dashed), and 30 km (solid line).

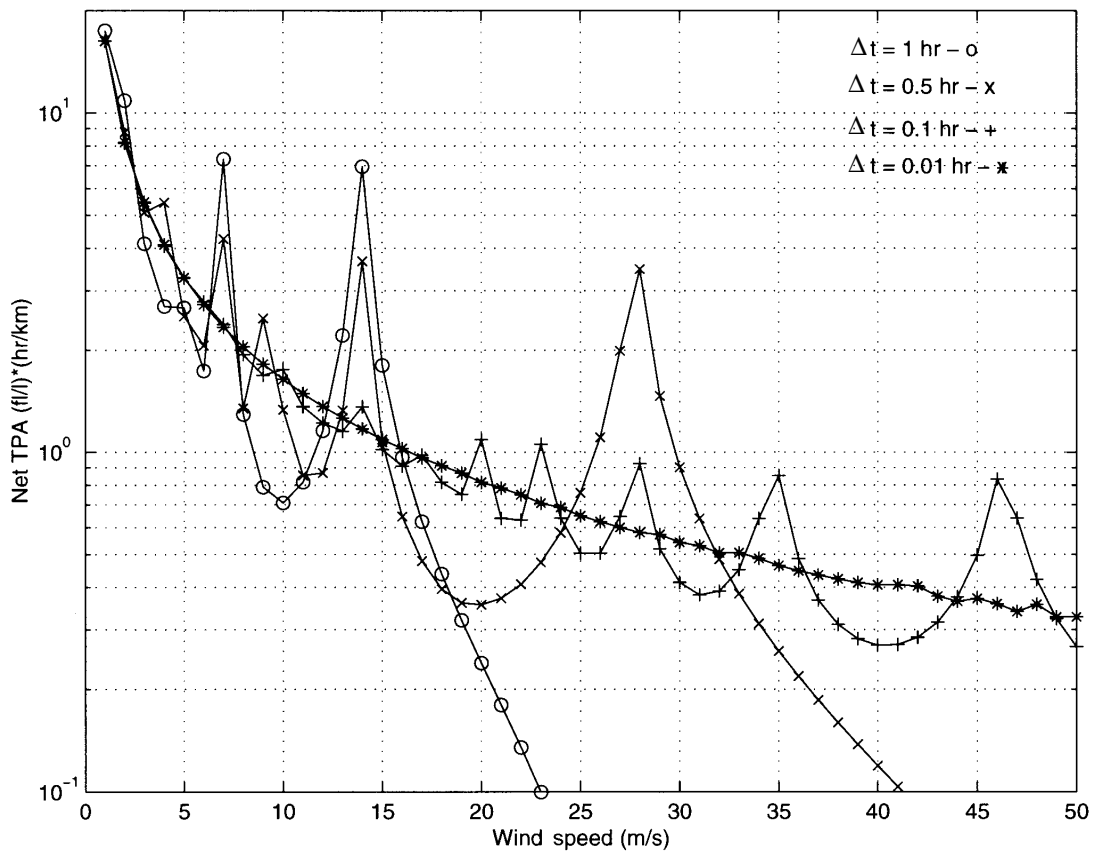


Figure 4. Net tracer potential area estimated for hypothetical example B (see text and Figure 3) as a function of wind speed. The discretization time increments are 1 (o), 0.5 (x), 0.1 (+), and 0.01 hour (*).

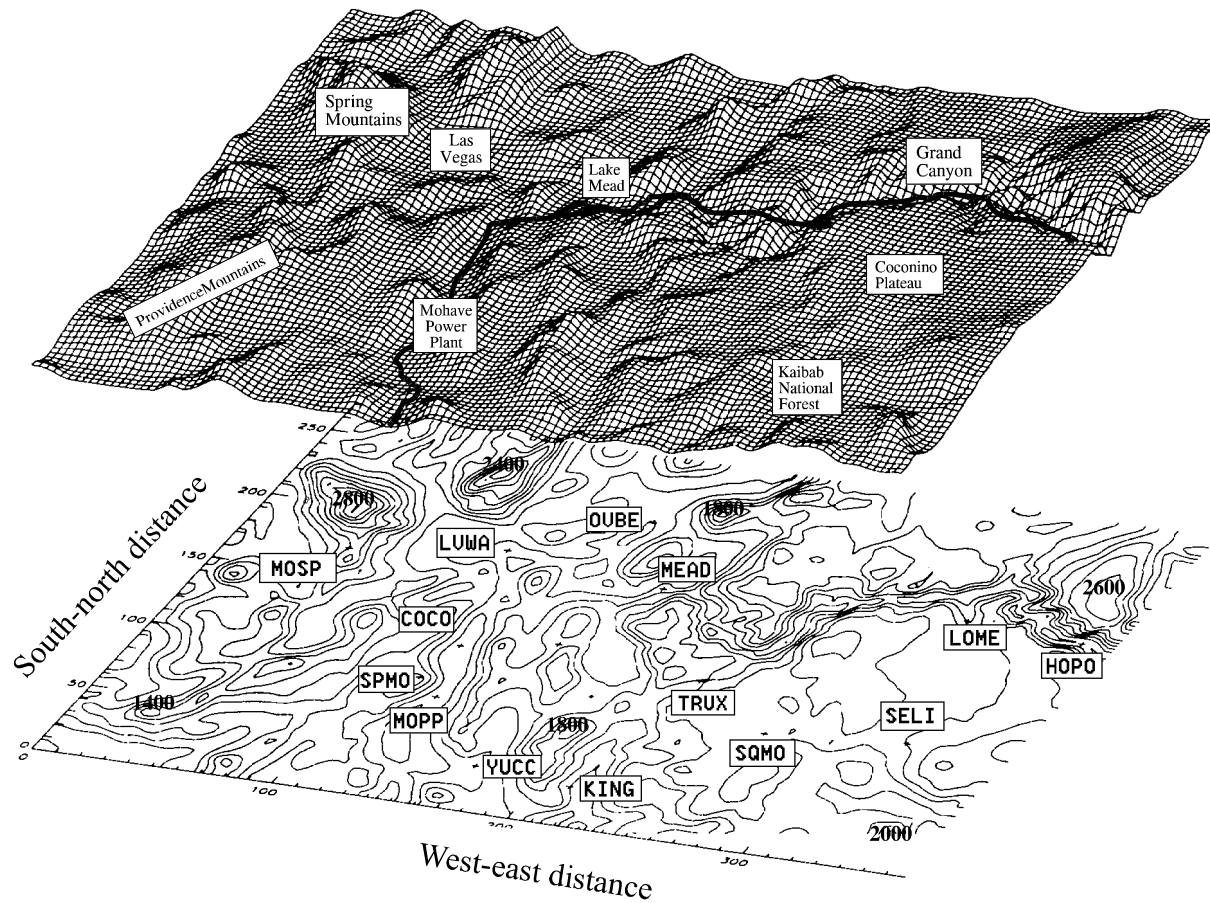


Figure 5. Topography of the Colorado River Valley area, centered at (35.7° N, 114.0° W), with source and receptor locations indicated. Contour interval is 100 m.

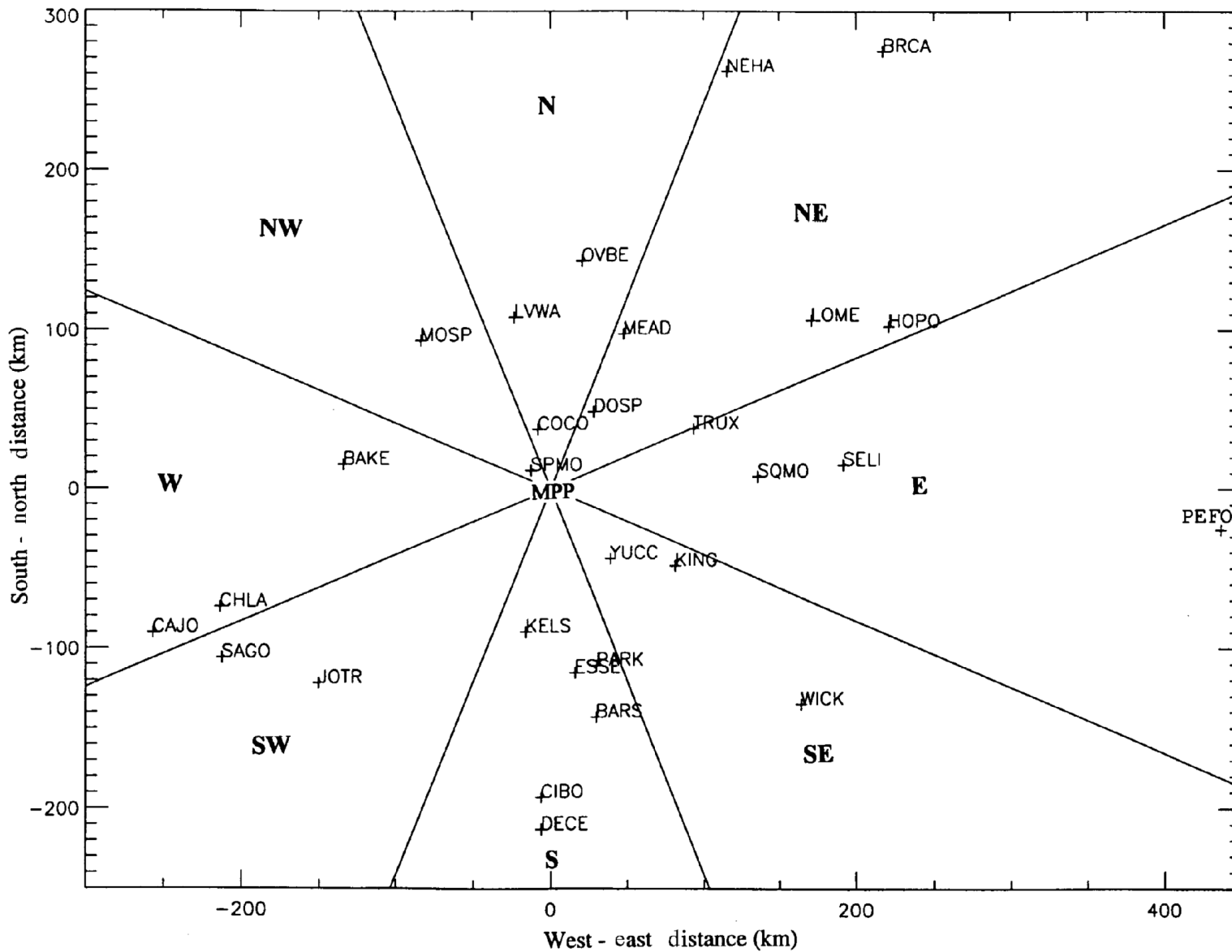


Figure 6. Positions of tracer receptors (see Table 2) in octants centered at the tracer release source (MPP).

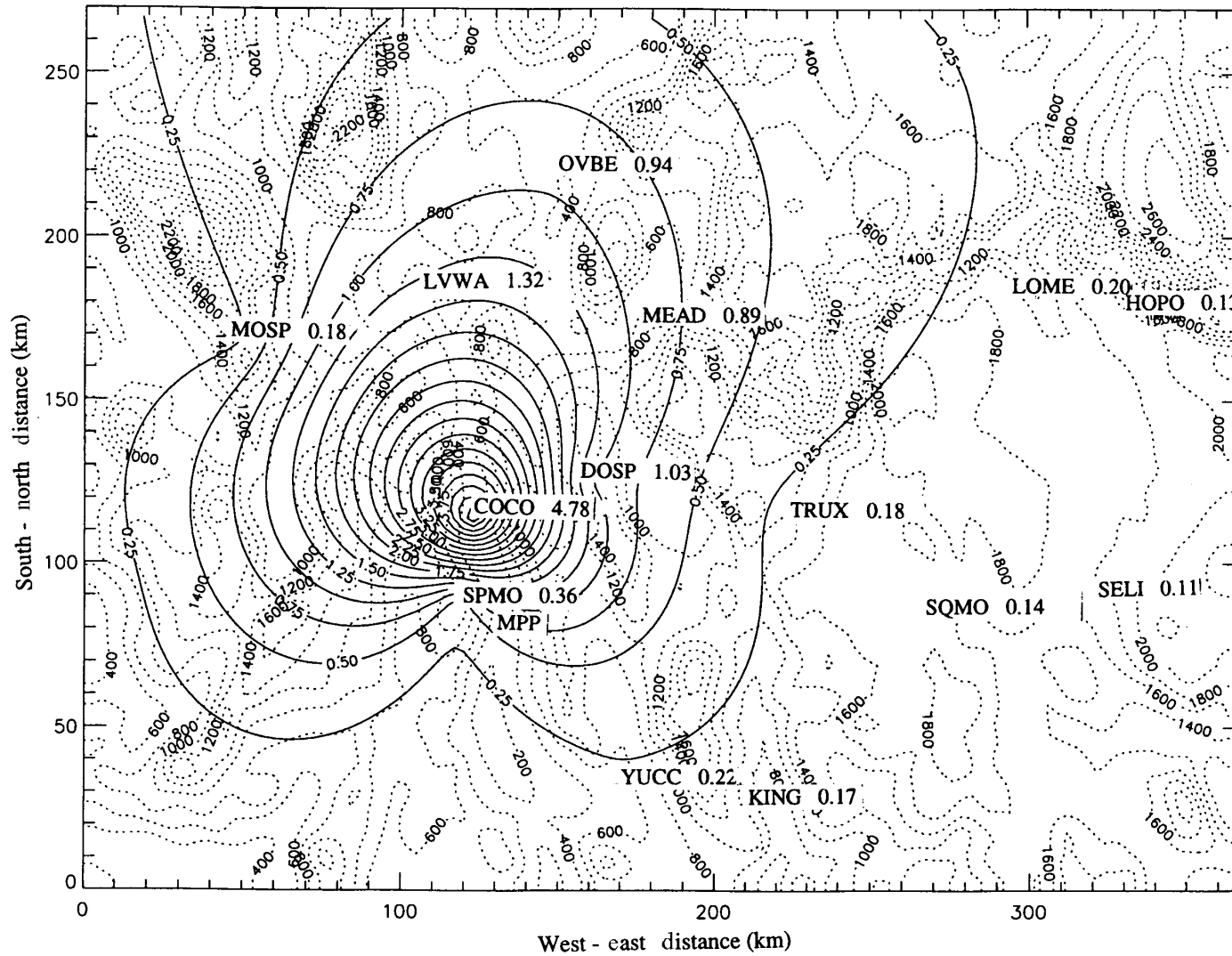


Figure 7. Contour plot of tracer concentration averaged over the period 5 July to 5 September 1992. Contour interval of tracer concentrations is $0.25 \text{ [fl l}^{-1}\text{]}$, and background contour interval of surface elevation is 200 m.

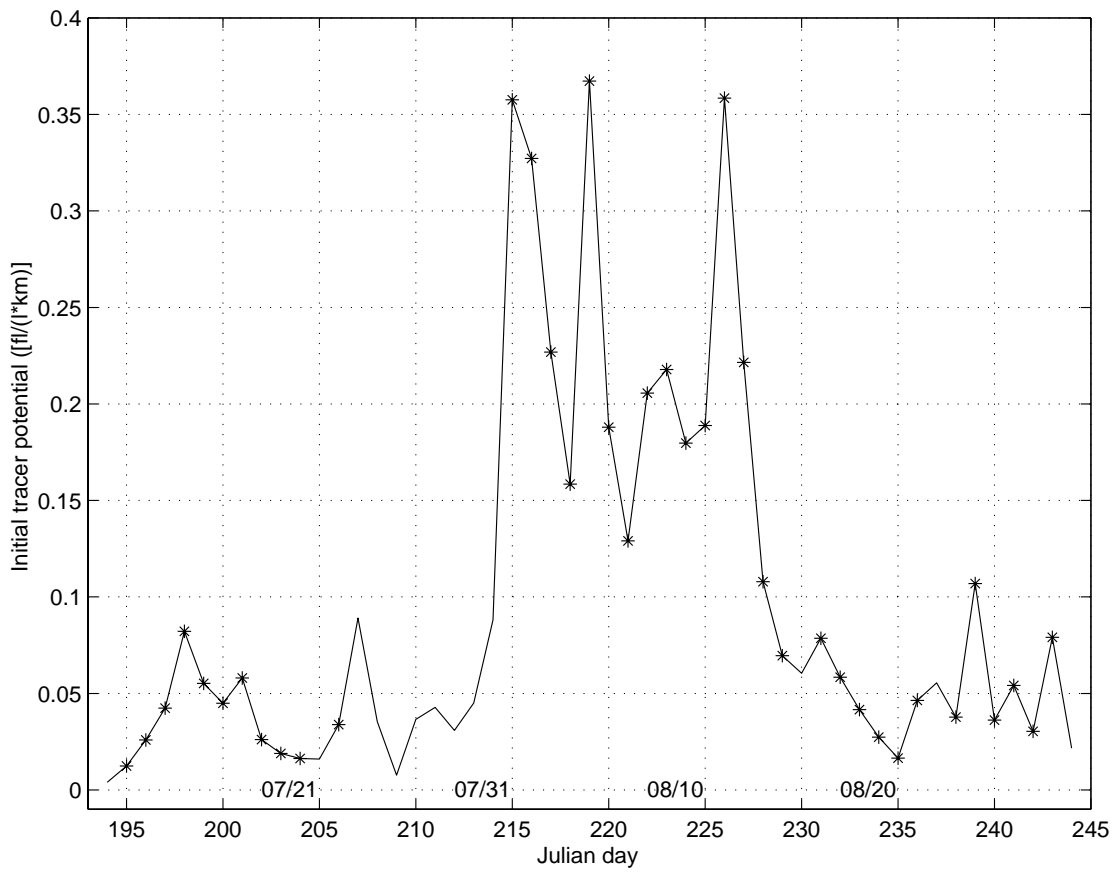


Figure 8. Time series of initial tracer potential for the studied area in summer 1992.

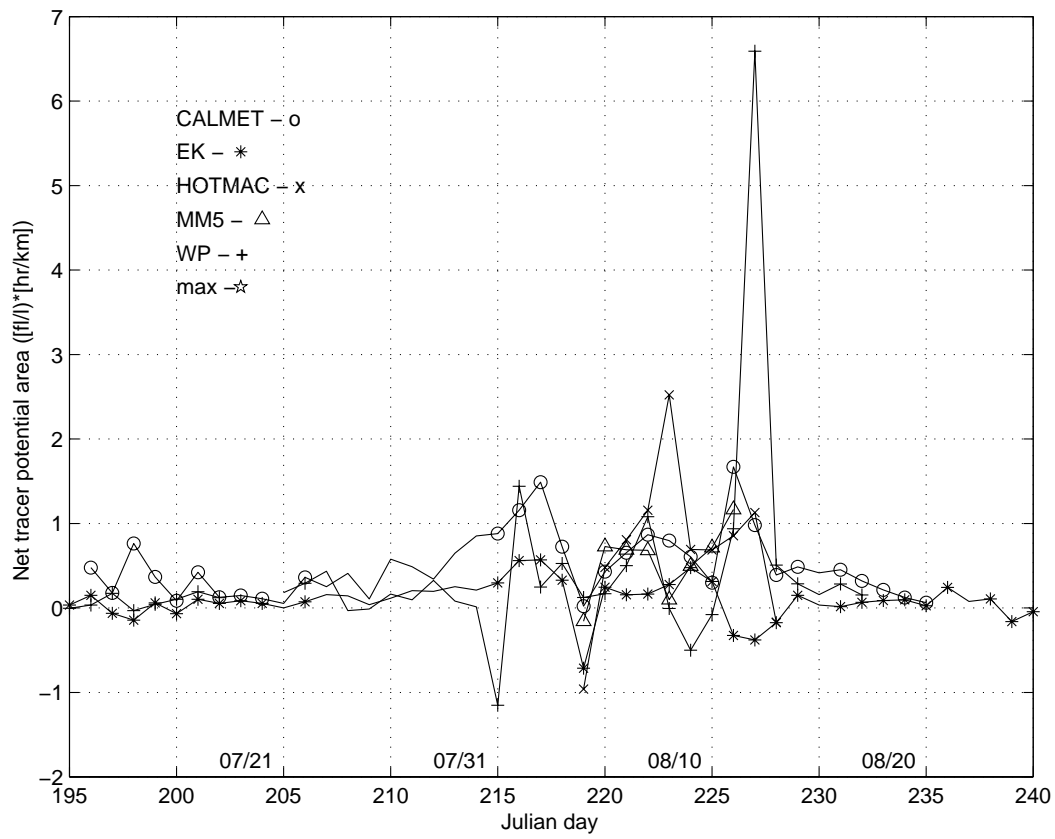


Figure 9. Time series of net tracer potential area for all wind fields for each day.

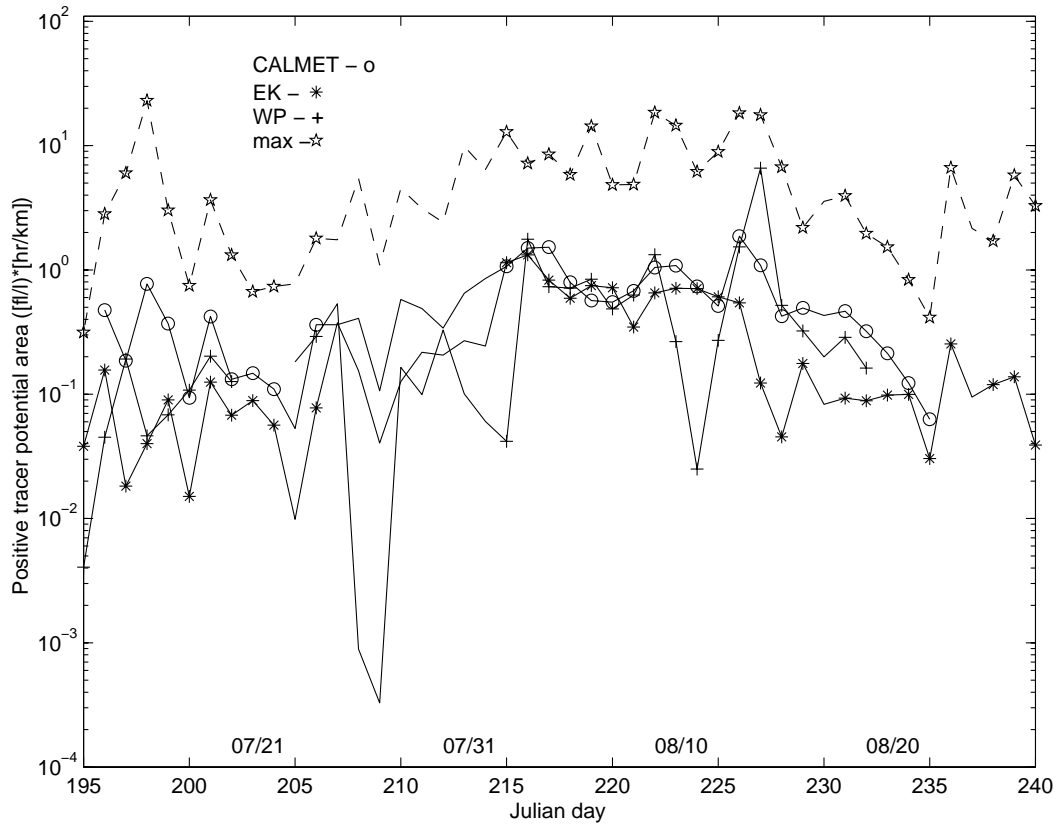


Figure 10. Time series of positive tracer potential area for CALMET, EK and WP wind fields (solid lines with indicated symbols) with estimated maximum net tracer potential area (dashed line) for each day.

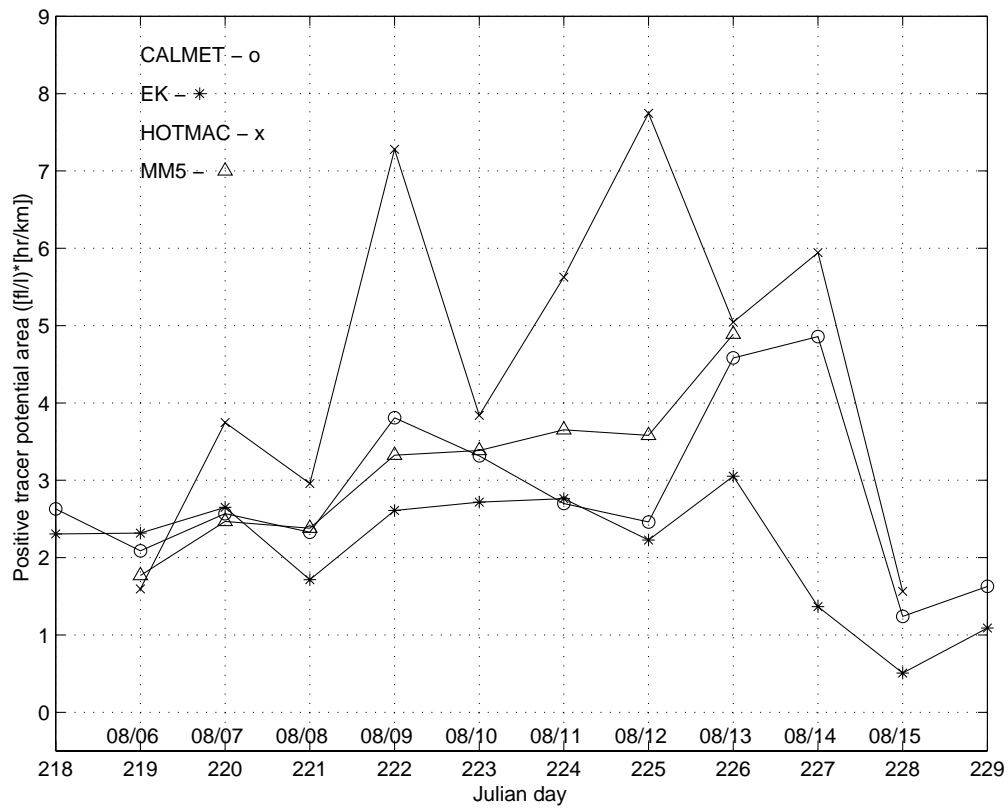


Figure 11. Time series of vertically-integrated positive tracer potential area for all available wind fields (solid lines with indicated symbols) with estimated maximum vertically-integrated positive tracer potential area (dashed line) for each day.

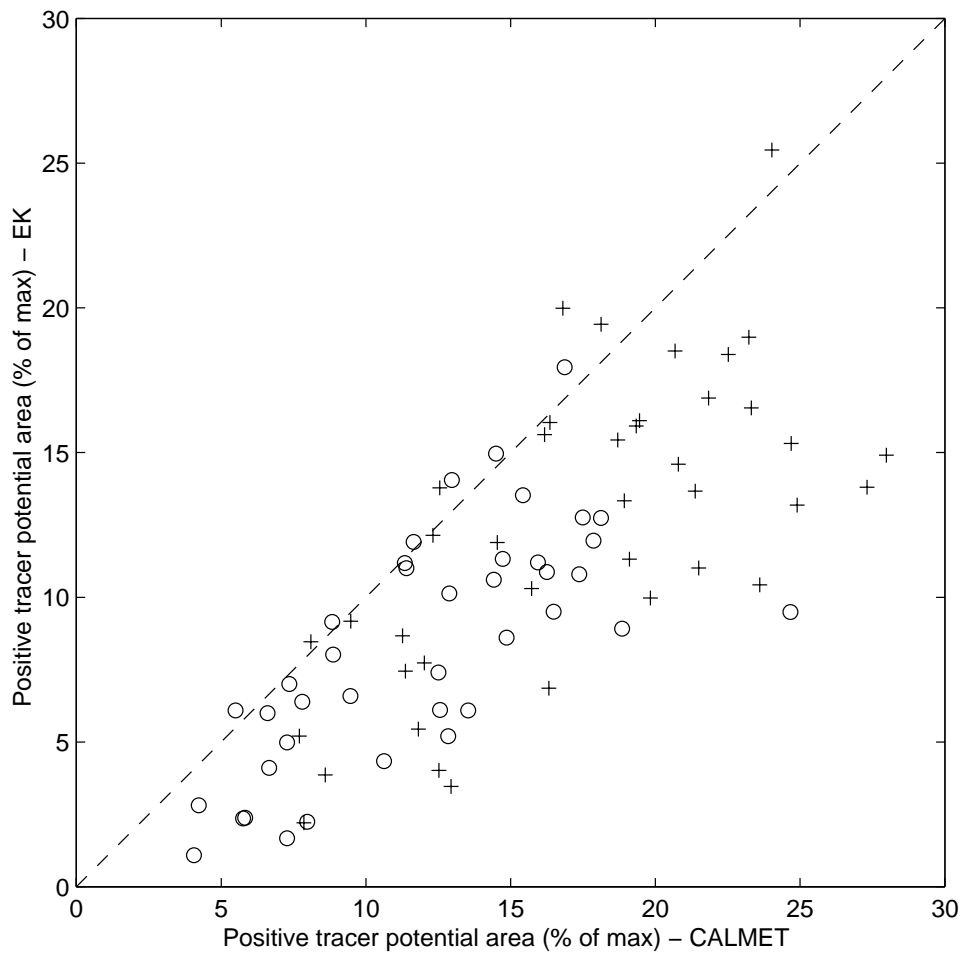


Figure 12. Scatter plot of the positive tracer potential area for CALMET and EK wind fields using inverse distance cost function (o) and inverse square-root distance cost function (+). Correlation coefficients are 0.77 and 0.76, respectively, and the number of points is 51 in each case.

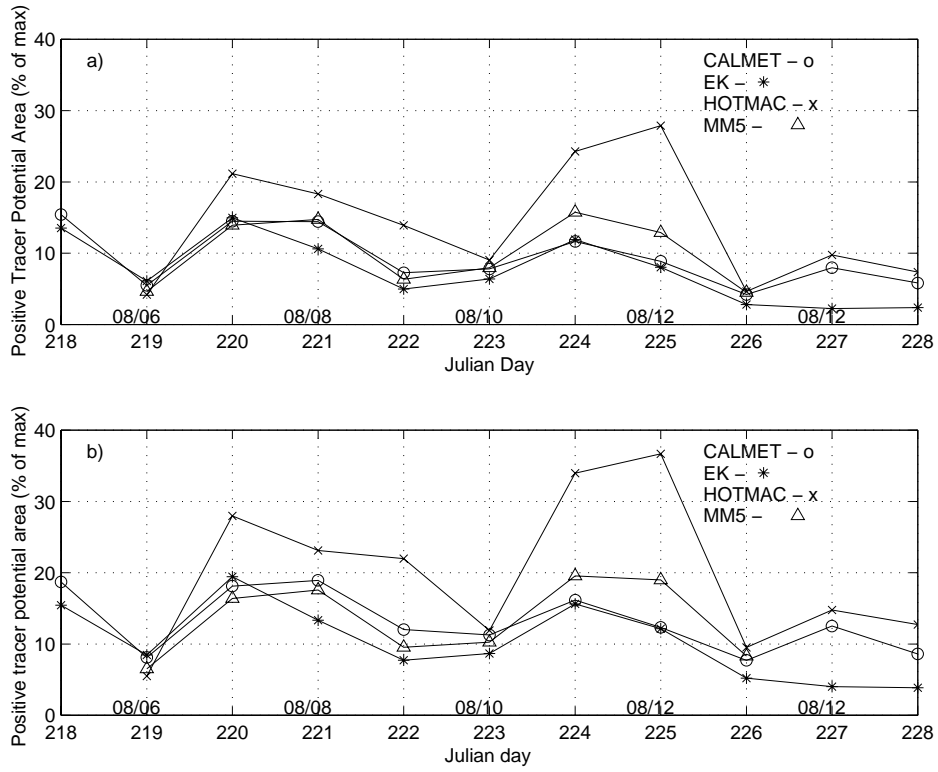


Figure 13. Time series of the positive tracer potential area for all available wind fields using different cost functions: inverse distance (a), and inverse square-root distance (b).

Table 1. Tracer receptor sites and their geographical locations.

Code	Name	Longitude (deg.)	Latitude (deg.)	Elevation (m)
BAKE	Baker, CA	-116.066	35.2833	283
BARS	Barstow, CA	-114.270	33.8600	590
BRCA	Bryce Canyon, UT	-112.166	37.6167	2438
CAJO	Cajon Pass, CA	-117.400	34.3333	1076
CHLA	China Lake, CA	-116.930	34.4800	2283
CIBO	Cibola NWR, CA	-114.660	33.4100	73
COCO	Cottonwood Cove, NV	-114.683	35.4833	274
DECE	Desert Center, CA	-114.660	33.2300	270
DOSP	Dolan Springs, AZ	-114.283	35.5833	853
ESSE	Essex, CA	-114.420	34.1100	520
HOPO	Hopi Point, AZ	-112.150	36.0667	2164
JOTR	Joshua Tree, CA	-116.233	34.0500	1250
KELS	Kelso, CA	-114.770	34.3400	860
KING	Kingman, AZ	-113.700	34.7100	1040
LOME	Long Mesa, AZ	-112.700	36.1000	1786
LVWA	Las Vegas Wash, NV	-114.850	36.1167	457
MEAD	Meadview, AZ	-114.067	36.0222	905
MOSP	Mount.Springs, NV	-115.516	35.9833	1753
NEHA	New Harmony, UT	-113.300	37.5000	1524
OVBE	Overton Beach, NV	-114.366	36.4333	396
PARK	Parker, AZ	-114.266	34.1500	137
PEFO	Pertified Forest NP, AZ	-109.795	34.9139	1690
SAGO	San Gorg.Wild., CA	-116.913	34.1933	1710
SELI	Seligman, AZ	-112.483	35.2833	1661
SPMO	Spirit Mount., NV	-114.733	35.2500	1498
SQMO	Squaw Mount., AZ	-113.100	35.2167	1981
TRUX	Truxton, AZ	-113.563	35.4861	1350
WICK	Wickenburg, AZ	-112.800	33.9333	732
YUCC	Yucca, AZ	-114.166	34.7500	579

Table 2. Receptors with distance and angle from tracer release source (MPP), and basic statistics of the tracer concentrations (C) measured during the field program.

Station code	Octant	Distance from MPP (km)	Direction (deg.)	Days operational	Mean C (f/l)	Std. C (f/l)	Median C (f/l)	Max C (f/l)	Uncertainty (%)
BAKE	W	134.9	277	54	0.06	0.09	0.05	0.66	11
BARS	S	145.9	168	43	0.05	0.03	0.05	0.10	11
BRCA	NE	350.2	38	29	0.25	0.14	0.21	0.65	7
CAJO	W	272.1	251	60	0.06	0.05	0.06	0.20	11
CHLA	W	226.0	251	20	0.03	0.01	0.03	0.05	11
CIBO	S	193.1	182	40	0.03	0.03	0.04	0.10	6
COCO	N	38.5	347	13	4.78	2.12	4.20	9.81	2
DECE	S	213.1	182	52	0.07	0.04	0.06	0.17	2
DOSP	NE	56.1	30	54	1.03	2.03	0.45	11.70	11
ESSE	S	116.2	172	55	0.26	0.87	0.05	6.19	11
HOPO	NE	243.3	65	61	0.14	0.13	0.09	0.50	9
JOTR	SW	193.5	231	40	0.07	0.04	0.07	0.12	6
KELS	S	91.0	190	56	0.10	0.12	0.07	0.71	5
KING	E	94.5	121	29	0.17	0.22	0.09	1.15	2
LOME	NE	201.2	58	16	0.20	0.25	0.10	0.70	8
LVWA	N	110.5	348	53	1.32	1.12	1.24	5.77	7
MEAD	NE	108.4	26	42	0.89	0.67	0.74	3.01	7
MOSP	NW	125.3	318	51	0.18	0.27	0.07	1.24	2
NEHA	NE	286.2	24	7	0.08	0.14	0.00	0.31	11
OVBE	N	144.6	8	50	0.94	0.80	0.79	3.13	11
PARK	S	114.6	165	37	0.03	0.03	0.02	0.10	11
PEFO	E	437.4	93	22	0.24	0.10	0.21	0.45	11
SAGO	SW	237.3	244	45	0.12	0.06	0.11	0.29	4
SELI	E	192.1	85	41	0.11	0.11	0.09	0.38	3
SPMO	NW	17.4	312	14	0.36	0.68	0.10	2.58	2
SQMO	E	135.7	87	33	0.14	0.15	0.08	0.67	11
TRUX	E	100.6	68	55	0.18	0.28	0.09	1.52	4
WICK	SE	212.3	129	21	0.21	0.17	0.17	0.82	11
YUCC	SE	58.6	139	51	0.22	0.61	0.08	3.19	4
Mean				39	0.42	0.39	0.32	1.94	7
Std.				16	0.90	0.55	0.80	2.93	4

Table 3. Number of operational receptors for each octant, mean differences in their angular positions, and initial TP for each day of the field program. A flag value of 0 means that at least one octant did not have an operational receptor; 1 means there was at least one operational receptor in each octant; and 2 means there were two or more operational receptors in each octant. The days selected for analysis are indicated in the last column.

	Date	Julian day	TPO [fl/(1*km)]	Total number	N	NE	E	SE	S	SW	W	NW	Mean angle [deg.]	St.dev. [deg.]	FLAG	Selection
1	12-Jul	194	0.0040	17	2	2	2	1	5	1	3	1	21	14	1	
2	13-Jul	195	0.0124	20	2	2	3	2	5	2	3	1	18	13	1	+
3	14-Jul	196	0.0259	21	2	3	3	2	5	2	3	1	17	13	1	+
4	15-Jul	197	0.0424	21	2	4	3	1	5	2	3	1	17	13	1	+
5	16-Jul	198	0.0822	21	2	4	3	2	4	2	3	1	17	13	1	+
6	17-Jul	199	0.0552	22	2	5	3	1	5	2	3	1	16	13	1	+
7	18-Jul	200	0.0449	22	2	5	3	1	5	2	3	1	16	13	1	+
8	19-Jul	201	0.0580	21	2	5	3	1	5	1	3	1	17	14	1	+
9	20-Jul	202	0.0261	22	2	5	3	2	5	1	3	1	16	13	1	+
10	21-Jul	203	0.0189	22	2	5	3	2	4	2	3	1	16	13	1	+
11	22-Jul	204	0.0163	21	2	4	3	2	4	2	3	1	17	13	1	+
12	23-Jul	205	0.0160	20	0	4	3	2	5	2	3	1	18	18	0	
13	24-Jul	206	0.0339	19	2	3	4	2	3	1	3	1	19	14	1	+
14	25-Jul	207	0.0891	15	3	3	1	1	2	2	2	1	24	18	1	
15	26-Jul	208	0.0354	10	2	3	1	1	1	0	2	0	36	31	0	
16	27-Jul	209	0.0077	6	2	2	0	0	1	0	1	0	60	38	0	
17	28-Jul	210	0.0366	7	2	3	0	0	1	0	1	0	51	41	0	
18	29-Jul	211	0.0428	7	2	2	0	1	1	0	1	0	51	31	0	
19	30-Jul	212	0.0309	7	2	2	0	1	1	0	1	0	51	31	0	
20	31-Jul	213	0.0450	8	2	4	0	0	1	0	1	0	45	42	0	
21	1-Aug	214	0.0881	15	2	5	2	1	3	0	2	0	24	22	0	
22	2-Aug	215	0.3576	21	3	4	2	1	5	2	2	2	17	14	1	+
23	3-Aug	216	0.3272	21	3	4	2	1	5	2	2	2	17	14	1	+
24	4-Aug	217	0.2269	21	3	4	2	1	5	2	2	2	17	14	1	+
25	5-Aug	218	0.1585	21	3	4	2	1	5	2	2	2	17	14	1	+
26	6-Aug	219	0.3673	20	3	4	2	1	5	2	1	2	18	15	1	+
27	7-Aug	220	0.1880	21	3	4	2	1	5	2	2	2	17	14	1	+
28	8-Aug	221	0.1291	22	3	4	2	2	5	2	2	2	16	12	2	+
29	9-Aug	222	0.2056	22	3	4	2	2	5	2	2	2	16	12	2	+
30	10-Aug	223	0.2179	22	3	4	2	2	5	2	2	2	16	12	2	+
31	11-Aug	224	0.1797	22	3	4	2	2	5	2	2	2	16	12	2	+
32	12-Aug	225	0.1888	22	3	4	2	2	5	2	2	2	16	12	2	+
33	13-Aug	226	0.3585	22	3	4	2	2	5	2	2	2	16	12	2	+
34	14-Aug	227	0.2215	20	2	4	2	2	5	2	1	2	18	12	1	+
35	15-Aug	228	0.1079	21	2	3	3	2	6	2	2	1	17	13	1	+
36	16-Aug	229	0.0696	21	2	3	3	2	6	2	2	1	17	13	1	+
37	17-Aug	230	0.0605	20	2	3	3	2	6	2	2	0	18	17	0	
38	18-Aug	231	0.0786	21	2	3	3	2	6	2	2	1	17	13	1	+
39	19-Aug	232	0.0584	21	2	3	3	2	6	2	2	1	17	13	1	+
40	20-Aug	233	0.0416	21	2	3	3	2	6	2	2	1	17	13	1	+
41	21-Aug	234	0.0274	18	2	3	2	2	5	1	2	1	20	15	1	+
42	22-Aug	235	0.0165	18	2	3	2	2	5	1	2	1	20	15	1	+
43	23-Aug	236	0.0464	18	2	3	2	2	5	1	2	1	20	15	1	+
44	24-Aug	237	0.0555	17	2	3	2	2	5	1	2	0	21	19	0	
45	25-Aug	238	0.0377	18	1	4	2	2	5	1	2	1	20	16	1	+
46	26-Aug	239	0.1069	18	1	4	2	2	5	1	2	1	20	16	1	+
47	27-Aug	240	0.0362	18	1	4	2	2	5	1	2	1	20	16	1	+
48	28-Aug	241	0.0541	18	1	4	2	2	5	1	2	1	20	16	1	+
49	29-Aug	242	0.0304	18	1	3	3	2	5	1	2	1	20	16	1	+
50	30-Aug	243	0.0791	18	1	3	3	2	5	1	2	1	20	16	1	+
51	31-Aug	244	0.0216	17	1	3	3	2	5	1	2	0	21	20	0	
Total				942	106	182	112	80	227	73	108	54				38
Percent				88	10	17	10	7	21	7	10	5				

Table 4. Daily percentages of success of each wind field in representing the tracer transport by using the vertically-integrated positive tracer potential area with respect to a maximum integrated positive tracer potential area (see text).

Date	Julian day	TP0	TP area max	CALMET	EK	HOTMAC	MM5
		[fl/(l*km)]	[(fl/l)*(hr/km)]	%	%	%	%
6-Aug	219	0.3673	38.03	5.5	6.1	4.2	4.7
7-Aug	220	0.1880	17.72	14.5	15.0	21.1	13.9
8-Aug	221	0.1291	16.16	14.4	10.6	18.3	14.7
9-Aug	222	0.2056	52.33	7.3	5.0	13.9	6.4
10-Aug	223	0.2179	42.50	7.8	6.4	9.0	8.0
11-Aug	224	0.1797	23.19	11.6	11.9	24.3	15.8
12-Aug	225	0.1888	27.77	8.9	8.0	27.9	12.9
13-Aug	226	0.3585	108.45	4.2	2.8	4.7	4.5